MSc Thesis in Applied Earth Siences

Determination of REV and Effective Properties of Fluvial Depositional Systems

Tim Lottman

2019

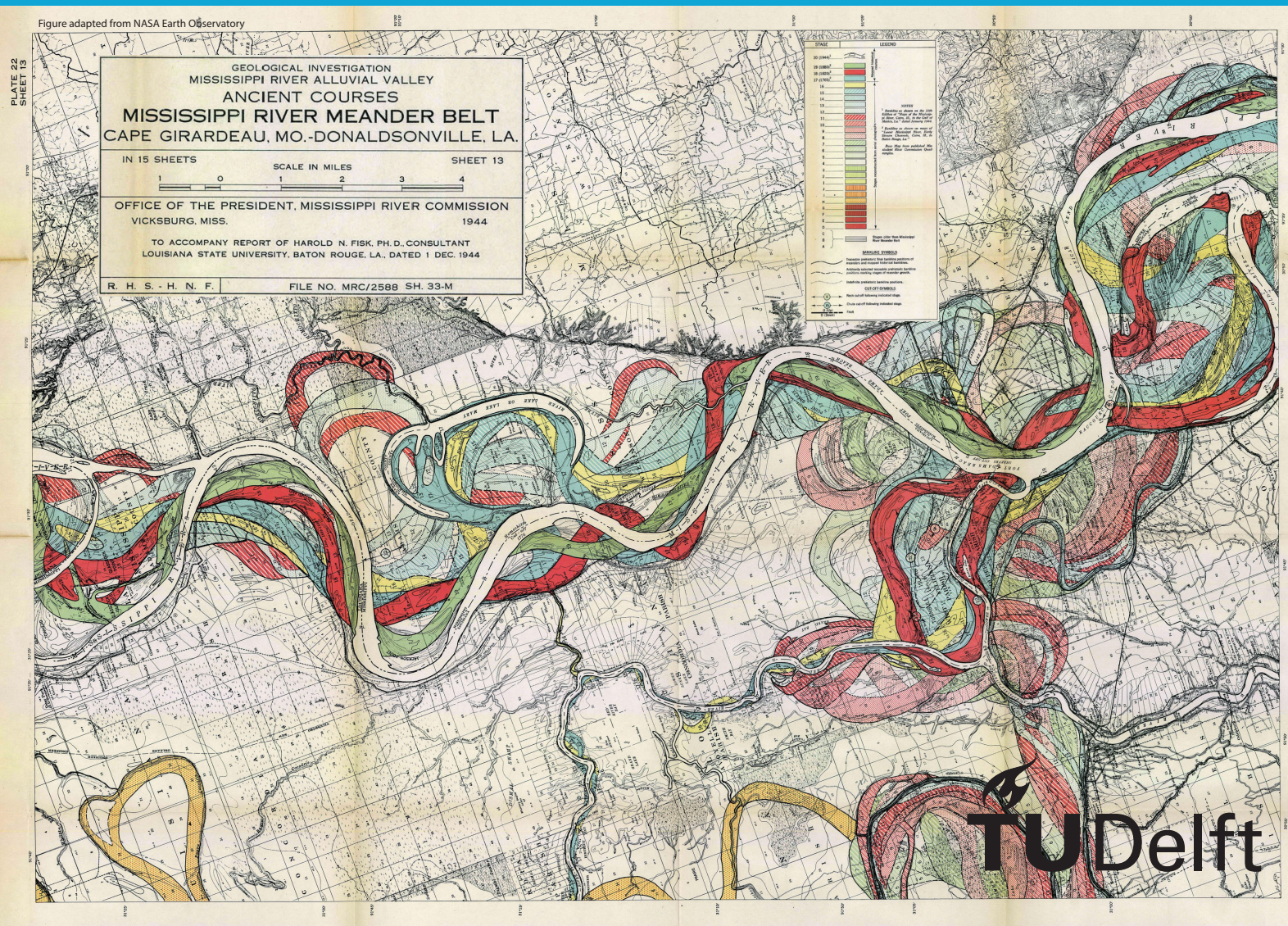

DETERMINATION OF REV AND EFFECTIVE PROPERTIES OF FLUVIAL DEPOSITIONAL SYSTEMS

A Feasibility Study Using 3D FLUMY® Models

A thesis submitted to the Delft University of Technology in partial fulfillment of the requirements for the degree of

Master of Science in Applied Earth Sciences

by

Tim Lottman

June 2019

Tim Lottman: *Determination of REV and Effective Properties of Fluvial Depositional Systems* (2019)
An electronic version of this thesis is available at:
http://repository.tudelft.nl/.

The work in this thesis was made in the:

Section Reservoir Geology
Department of Applied Geology
Faculty of Civil Engineering & Geosciences
Delft University of Technology

Supervisors:	Dr. J.E.A. Storms	Associate Professor TU Delft
	Prof. Dr. A.W. Martinius	Professor TU Delft/Equinor
Committee:	Dr. ir. F.C. Vossepoel	Associate Professor TU Delft
	Dr. ir. K. Nordahl	Equinor

ABSTRACT

Fluvial reservoirs are difficult to model due to the high permeability contrast between the sandstone bodies and the overbank deposits and the complex geometry of the permeable (sandstone bodies) and impermeable zones (overbank deposits). A set of fluvial meandering models has been generated using FLUMY®. The models represent a range of Net-to-Gross ratios and sandstone body geometries. In order to quantify the effect of sample size on effective properties, the models are evaluated based on the statistical moments of the probability distributions of porosity and single-phase permeability as a function of sample size. The porosity and permeability show a high spread at small sample volumes, but the spread reduces as the sample size increases. A normalized standard deviation, the coefficient of variation, has been used as a criterion for the variability of the probability distributions. The coefficient of variation of the porosity and the horizontal permeability show a monotonic decline as a function of sample size. The coefficient of variation of the vertical permeability does not show a monotonic decline. This is caused by a drastic decrease of the mean of the vertical permeability with increasing sample volume. The mean of the horizontal permeability also decreases with increasing sample size, but to a lesser extent. The mean of the probability distributions of permeability as a function of sample size converges much earlier than the standard deviation. This convergence indicates that we can determine the effective properties at the Representative Elementary Volume (REV), without reaching REV. The convergence of the mean could potentially be used as a criterion for the relevant spatial scale of upscaling from the fine scale static model to the coarse scale model. Furthermore, if cells are uncorrelated at a scale where the mean of the permeability is not a function of sample volume anymore, random attribution of properties can be used to populate dynamic grid cells.

ACKNOWLEDGEMENTS

First of all, I would like to thank my supervisor Joep Storms for his support, help, guidance and especially patience during my (too) long and often unstructured disquisitions. The help with structuring both my thoughts and writing was invaluable for finalizing this thesis.
Secondly, I would like to thank Allard Martinius for a lot of valuable insights during our meetings. His insights about REV theory and the applications that have been used and developed at Statoil/Equinor formed the backbone of my thesis. Although we did not meet regularly, he asked the right questions and mentioned the missing links in this thesis.
I would like to express my gratitude to Kjetil Nordahl without whom I would not have been able to finish this project. His work on REV and determination of effective properties of fluvial deposits formed the backbone of his thesis. Without his ideas, I would never have the results and insights that I have obtained now.
I would also like to thank Femke Vossepoel for being part of my committee. Her involvement during the final part of my study helped me with structuring my report and improve my scientific writing.
At this point, I would like my family for all the love and support that I have received to the point of finalizing my studies. I would like to highlight my parents that have unconditionally supported me both emotionally, with a 'kick in the butt' when needed, and financially during my studies.
I would like to thank Robyn for being my love and care during the last year of my study. I will be happy if we have both finalized our studies and approach a new step in life.
Finally, I would like to thank all my study friends. I would never have been able to finalize this report without the lunch and coffee breaks at the faculty!

CONTENTS

LIST OF FIGURES

LIST OF TABLES

1 INTRODUCTION

1.1 RESERVOIR MODELING

Subsurface resources such as oil, gas and water are generally recovered from porous and permeable (either by initial permeability of the rock itself or artificially created permeability) rock layers. Permeable rock layers contain one or multiple fluids or gasses within the matrix[1]. A porous and permeable rock layer that contains a subsurface resource is called a reservoir. Wells are drilled into the reservoir to extract the fluids or gasses from the surbsurface if it is not in direct contact with the surface. In order to predict the amount of available and extractable resources and to determine the response of the reservoir on the extraction of resources by the wells, a model of the reservoir is built. This model tries to capture the often complex interaction between the matrix and fluids/gasses. The high uncertainty, between the actual state of the reservoir and the modelled one makes reservoir modeling a difficult task. Still, reservoir modeling forms an important tool to evaluate the various stages of field development. Reservoir models are built and evaluated over the entire life of the reservoir. According to Howell et al. (2014), they are important during various stages of the field development:

- Field appraisal and development, for optimizing well location and spacing.
- Production, monitoring and predicting performance and planning infill wells (Labourdette, 2008).
- Prior to Enhanced Oil Recovery[2], predicting the performance and evaluate economic viability (Matthews et al., 2008).
- Decommissioning, to demonstrate regulators and stakeholders that the field is ready to be abandoned (Ruivo et al., 2001).

Reservoir models can generally be divided into two model groups. Geological or static models, created by geologists and geophysicists (that depict the geology of the reservoir in a static model) and reservoir simulation models that use the static model to simulate the flow of fluids through the reservoir over time based on properties such as porosity, permeability and water saturation. The focus of this research is on the population of the reservoir properties of the static model and the dynamic model is therefore not further discussed.

1.1.1 The Static Reservoir Model

A static reservoir model depicts the physical space of the reservoir by an array of discrete (regular or irregular) cells. Static reservoir models aim to integrate data from a broad range

1 The matrix is the solid part of the reservoir and bounds the void space that is able to contain or transmit fluids or gasses.

2 Enhanced Oil Recovery (EOR) or tertiary oil recovery are methods that are used to obtain more or faster production of oil from the reservoir by use of gas, thermal or chemical injection into the reservoir. The main goal of EOR is to increase the mobility of oil in order to enhance extraction.

of measurements (Figure 1.1) to capture both a geologically realistic range of measurements and the spatial variability of in petrophysical properties (Keogh et al., 2007). An important purpose of a static reservoir model is to serve as a high fidelity scale input for dynamic reservoir simulations models, so as to be able to realistically simulate flow through them. Keogh et al. (2007) state that: "Reservoirs have potentially measurable, deterministic properties at all scales that arise from the interaction of many, complex processes and are therefore intrinsically deterministic in nature." This observation is important, because it implies that all "errors" and uncertainties in static geological models arise either from lack of data or lack of computational power to represent all details present in the actual reservoir. In particular the data that we sample from the reservoir is incomplete and of different resolution (vertical and horizontal) (Keogh et al., 2007). One can generally say that the data that is sampled increases in resolution with a decrease in data covered as a percentage of the entire reservoir (Figure 1.1).

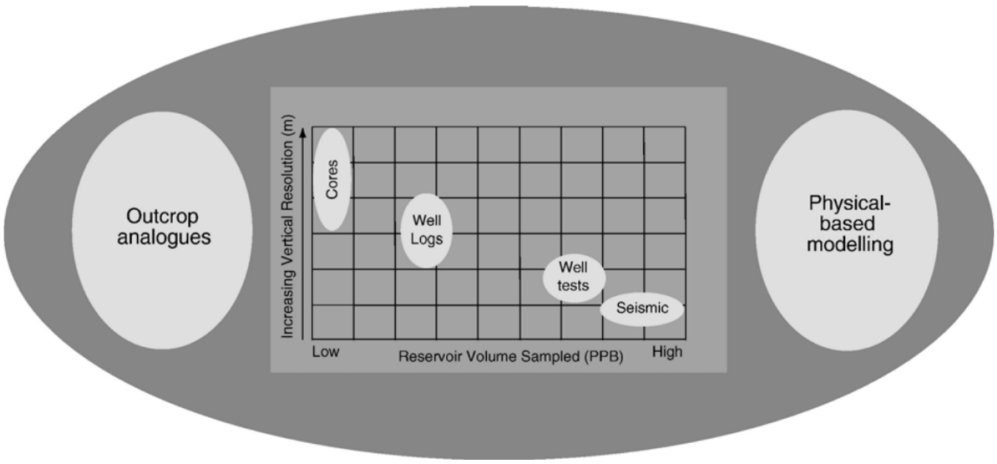

Figure 1.1: A chart showing the subsurface data types that are used as input to construct reservoir models. The reservoir volume sampled is plotted against the vertical resolution of the data type. Outcrop analogues and Physical-based modeling techniques can be used to link the different data sources and construct more realistic models (Keogh et al., 2007).

1.1.2 Reservoir Architecture and Spatial Modeling

The geological features of the model can be classified as external and internal geometrical features. External features include information like trap configuration, seal capacity and the base of the reservoir. The internal geometry of the reservoir (reservoir architecture) is related to the 3D (or 2D) distribution of lithofacies in the reservoir. Lithofacies are a mappable subdivision of a stratigraphic unit that can be distinguished by its properties like texture, mineralogy, grain size and depositional environment that produced it. The lithofacies can be translated to petrophysical properties, such as porosity and permeability, that are used as input parameters for the static and dynamic models. Reservoir architecture (internal geometry) has heterogeneities at multiple scales. Especially fluvial reservoirs, which is the focus of this study, are often challenging due to the complex nature of the geometry and distribution of the sandstone bodies (Pettijohn et al., 1973; Nordahl and Ringrose, 2008; Keogh et al., 2014) and the large contrast between the petrophysical properties of sandstone bodies and over-

bank deposits. These deposits are unsuited to be modelled with simple trend mapping and interpolation techniques (Keogh et al., 2007). This is due to the heterogeneity levels of fluvial reservoirs. Heterogeneity of fluvial reservoirs can be characterized by hierarchical scales (Weber, 1986; Haldorsen, 1986; Nordahl and Ringrose, 2008; Ringrose et al., 2008)(Figure 1.2). Since it is impossible to model every scale of heterogeneity, 3D cell arrays are used to model the different properties of the reservoir and represent the static and dynamic properties of the interval averaged over the cell. Properties can be represented as both scalar and tensor fields in Euclidean space (2D or 3D). Especially spatial distribution of lithological heterogeneity is of main importance for proper static and dynamic reservoir modeling.

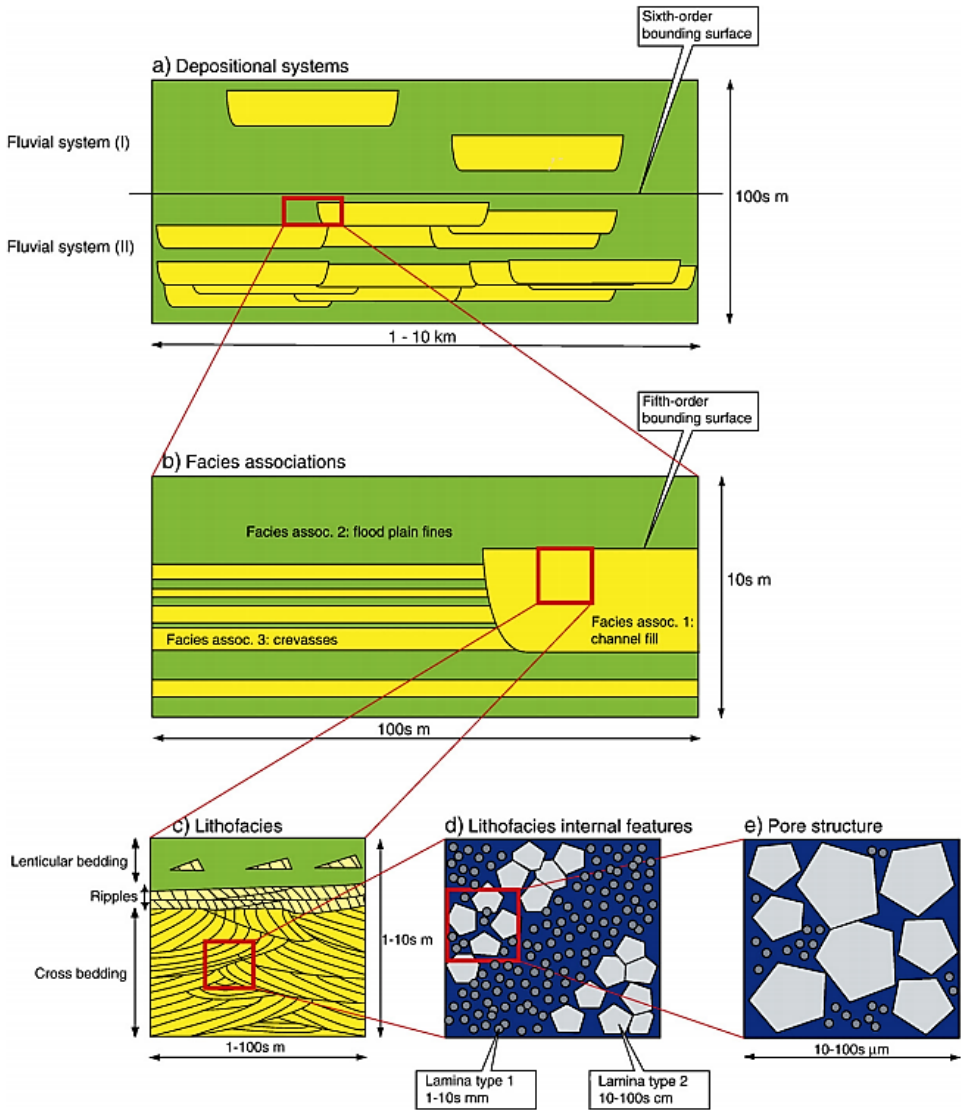

Figure 1.2: A schematic view of different scales and heterogeneities that affect the properties of a reservoir in a fluvial depositional system. Pettijohn et al. (1973) proposed this hierarchical sequence of heterogeneity types. Figure based on Keogh et al. (2014) after Haldorsen (1986).

1.2 THE *continuum approach* IN POROUS MEDIA

The reservoir can be seen as a complex interaction of static (grains, cement) and dynamic (water, oil, gas) particles. If we want to model a very simple homogeneous sandstone (solid phase) with water and black oil below bubble point (liquid phases), it is almost impossible to describe this in terms of the intermolecular interactions. Even more, if an extensive quantity of a phase is modeled in terms of the state variables at points inside the domain that is occupied by the phase where the interphase surfaces act as the boundaries (Bachmat and Bear, 1987), it is still a very cumbersome task to model this in a porous sandstone that generally has very complex geometries. Simplifications of pore models exist where this can be analytically solved (e.g., Kozeny-Carman's equation that models the void space as multiple tubes with varying diameter (Kozeny, 1927; Carman, 1937), but the formula has empirically tested factors to correct for tortuosity and geometry of the fluid pathways). Recent developments in micro-scale pore-structure characterization are promising (e.g. Chen et al., 2013; Jungreuthmayer et al., 2015; Tsuji et al., 2016), but this is not a generally applied method (yet). A widely accepted and used method is the *continuum approach*. In the continuum approach, a passage is made from the microscopic description to the macroscopic description. In the macroscopic description, a value is assigned to the state variables of all phases that are present in the investigated porous medium domain (Bachmat and Bear, 1986). One of the most obvious variables in the case of a porous medium is the presence of two persistent subdomains: the solid phase and void space. The volume of the voids devided by the the total volume of the sample space is expressed as the porosity (ϕ), a property that inevitably arises from the *continuum approach*. The *continuum approach* is also referred to as the effective medium approximation and is a widely used method in the oil and gas industry.

1.2.1 The *Continuum Approach* and Elementary Volumes

The inability to describe the the processes in porous media at the microscopic level leads us to adopt the *continuum approach*. The real porous medium is then replaced by a fictitious model, a continuum that fills up the entire area/volume of the phase. These area's/volumes are referred to as *elementary area's/volumes* (EA's/EV's). One or a set of continua can be averaged over this EA/EV and assigned to the centroid of the EA/EV. One can select any *Arbitrary Elementary Area/Volume* (AEA/AEV) from passing from a microscopic description to a macroscopic description of the system. Bachmat and Bear (1986) states that: 'Obviously, different AEV's will yield different averaged values for each quantity of interest, and there is no sense in asking which of them is more 'correct'.' However, since a value may strongly depend on the size of the volume over which it was taken, it must be labelled by the size of the AEV/AEA. In order to avoid this labelling of AEV's and a find a more generic value for the macroscopic description, Bear (1972) introduced the concept of a representative elementary volume (REV). Hubbert (1956) already realized that the length scale of re-scaling in the *continuum approach* is essential to obtain a generic value that is meaningful in the macroscopic description of a porous medium. In order to quantify the representativeness of the re-scaling size using the *continuum approach*, Bear (1972) states that a Representative Elementary Volume (REV) is a re-scaling volume that is both homogeneous (within a prescribed error level) and statistically stationary (i.e. the joint probability distribution does not change over location) (Nordahl and Ringrose, 2008) within the investigated domain. Figure 1.3 shows a hypothetical sample of a porous medium. The red squares are arbitrary elementary area's (AEA) that sample a desired property from the domain. If the AEA is small, the measured property is heavily dependent on the location of the elementary area. If the area increases, the chances of capturing a representative amount of the heterogeneity of the sample increase and could converge to a value that is representative for the sample as a whole. The elementary areas (or

volumes) within the range that reach a value that does not change with location, within a prescribed error level, is called the representative elementary area (REA) or in 3 dimensions representative elementary volume (REV) (Bachmat and Bear, 1986). Although the concept of REV is quite clear and straightforward, quantification and implications of REV are often very difficult/impossible to obtain. The main area of interest for REV quantification is the shift from the microscopic scale (pores and grains) to the macroscopic scale (core plugs, tube flow experiments). In geology, we generally talk about the porosity, absolute permeability, kv/kh-ratio[3], etc. of a particular type of rock, like they are properties that evidently arise from a single measurement of the rock. One of the main reasons for this is that we generally assume a core-plug to be of a fairly homogeneous rock like *Bentheim Sandstone*[4]. A *Bentheim Sandstone* core plug is indeed at REV at the scale these measurements are taken. This is not the case for all core plug measurements from rocks. Corbett and Jensen (1992) and Nordahl et al. (2005) showed that conventional core plugs are often not at an appropriate scale for determining representativity. A way industry deals with the variability of the measurement is by using arithmetic/geometric/harmonic averages and probability distribution of a set of measurements. They populate the model with the statistical properties of the dataset. This method could be adequate if the cells that are populated are the same size at which the measurement was taken (although more objections exist which are addressed in chapter 4). If we use larger sized cells, the shape and width of the probability distribution (and possibly the mean) of the modeled property will differ from the probability distribution of the small scale measurement (generally σ decreases and the shape will tend to go from a log-normal towards a normal distribution (Nordahl et al. (2014)). Using the REV of the measurement's heterogeneity scale will (partially) avoid these probability distribution scaling problems, since it is by definition representative for the scale of that heterogeneity.

1.2.2 The Representative Elementary Volume of Fluvial Reservoirs at the Scale of the Depositional System

Pettijohn et al.'s (1973) observations about heterogeneity scales are around for decades, but the re-scaling sizes we use are mainly based on the data that we can obtain from the reservoir (Figure 1.2). Haldorsen (1986) defines four main scales that are used for re-scaling:

- *Microscopic scale*, the scale of pores and grains.
- *Macroscopic scale*, the scale of conventional core plugs.
- *Megascopic scale*, the scale of large grid blocks in simulation models.
- *Gigascopic scale*, the scale of the depositional system/reservoir.

These scales can be subdivided into multiple sub-heterogeneity scales. Apart from the use of REV in the passage from the microscopic scale to the macroscopic scale, the last two decades much research has been done on multi-scale modeling (Ringrose et al., 2008; Howell et al., 2014; Nordahl et al., 2014). In the multi-scale modeling approach, the reservoir property distributions[5] are related to the measurement property distributions. REV serves an important role in this approach, since it gives better representations of the effective permeability architecture (Nordahl et al., 2014). The main area of interest for REV determination in multi-scale modeling is the sub-meter scale. Primary sedimentary structures significantly influence flow properties (Hartkamp-Bakker and Donselaar, 1993; Weber, 1982; Hurst, 2009), but it is

3 Vetical permeability devided by the horizontal permeability.
4 An Early Cretaceous shallow-marine homogeneous sandstone that forms an important reservoir rock in the Dutch/German subsurface.
5 Probability distribution of a property of the grid cells in a static/dynamic reservoir model.

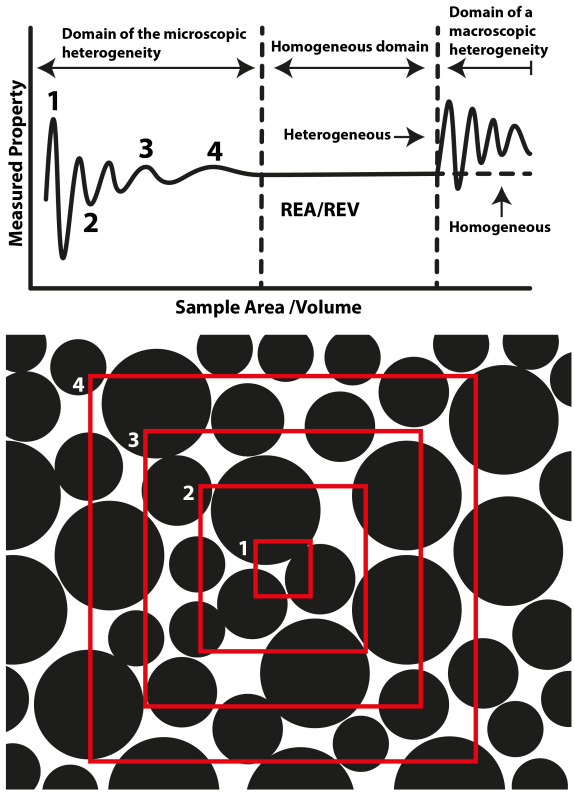

Figure 1.3: Arbitrary elementary area's (AEA) in the passage from a microscopic description to a macroscopic description of the system. The graph shows the relation of an area to the measured macroscopic property of the AEA. The smallest arbitrary area that approaches any property that is representative for the system as a whole (i.e., the value does not change significantly if the sample volume increases) is referred to as the representative elementary area (REA) for that specific property. The same holds for arbitrary elementary volumes (AEV) and representative elementary volumes (REV) (After Bachmat and Bear (1986)).

impossible to include them explicitly in a full-field reservoir model due to computational limitations (Nordahl and Ringrose, 2008). Additive properties (porosity) may be up-scaled with averaging schemes whilst non-additive properties (permeability) have to be represented by realistic models with heterogeneities included explicitly (Nordahl and Ringrose, 2008). Exact solutions are available in the case of simple geometries like stratified media, but sedimentary geometries are generally more complex. Multiple methods have been used for estimation of effective properties (effective media theory (Dagan, 1979), percolation theory (Begg and King, 1985) and deterministic modeling of sedimentary structures (Corbett and Jensen, 1992; Ringrose et al., 1999). Nordahl and Ringrose (2008) showed that it is possible to use tidal lithofacies models generated in SBED^{TM} to obtain REV sizes and do statistical analysis of permeability based on the sample size of a lithofacies model. These results raise questions if it might be possible to do REV analysis on larger re-scaling sizes such as from the microscopic scale to the megascopic scale or from the megascopic scale to the gigascopic scale.

1.3 RESEARCH GOALS

The goal of this research is to evaluate if it is possible to determine the Representative Elementary Volume and the effective properties of fluvial depositional systems. Much research has been done on relevant spatial scale of fluvial reservoirs (Nordahl and Ringrose, 2008; Keogh et al., 2014; de Hoop, 2017), but modeling of these reservoirs, with often complex geometries, is difficult. The use of REV theory has proven to be successful for modeling of small scale heterogeneities in sedimentary deposits with a high permeability contast (Nordahl and Ringrose, 2008; Keogh et al., 2014). This raises the question if it is possible to use the same approach for upscaling of the cells at the scale of the reservoir. The fluvial models are generated using FLUMY®. Synthetic data is used, because limited real world data exists with the detail needed for the research. Theoretically, REV is reached when the coefficient of variation of a property (porosity, permeability) is zero and the mean does not vary with sample size. The coefficient of variation will always approach zero if the sample size increases and the sample space is infinitely large. A property value (porosity, permeability) at which the amount of dispersion is small enough to be considered at REV is therefore disputable. It is therefore avoided to make statements about the point where the REV is reached. Rather does this study investigate relations between geometrical properties of the models and the influence on the statistical moments of the probability distributions at different sample sizes. Furthermore, it is investigated whether the effective permeability at the size of the REV can be determined without sampling at the REV scale.

The main research questions are:

- Is it possible to do REV analysis on models of fluvial depositional systems?
- Is it possible to find the effective permeability at REV based on the statistical moments of probability distributions as a function of sub-sample size?
- Is it possible to relate simple properties such as Net-to-Gross and sandstone body geometry to the effective properties and the size of the REV of a fluvial depositional system?
- Does REV analysis of models of fluvial depositional systems have (potential) applications for modeling of fluvial reservoirs?

2 METHODOLOGY

2.1 GENERATION OF NUMERICAL MODELS OF FLUVIAL DEPOSITIONAL SYSTEMS

A REV can be determined based on real sedimentary rock data, numerical data and even qualitative data like geological drawings. A REV is desirably determined based on real life data. The use of real sedimentary data from smaller samples is possible although time consuming, but it is impossible at reservoir scale, since no such data exists. Process-based and stochastic models of the subsurface provide a solution to generate physically realistic sedimentary deposits and are able to generate a model in three-dimensional space. To determine the REV at the scale of the fluvial system, a realistic input model is needed. The main attributes needed to obtain a proper model are:

- A geologically realistic spatial distribution of the channels in three dimensional space.
- A geologically realistic channel development resulting in the deposition of architectural elements like point bars, levees, abandoned channels, alluvium and crevasse splays.
- A sample space that is large enough to get samples that can be used for the determination of the REV.
- Grid cells that are small enough to be representative for the heterogeneity and geometry of the architectural elements, but large enough to run averaging functions and flow-based upscaling simulations.
- A large variety of models with different systems to be able to compare these systems and make (more) general conclusions.

These attributes make it impossible to generate data from real world reservoir, since the amount of detail needed is too small for the resolution of the data gathered from the reservoir. Analogues can be used to compute the architectural elements of the reservoir using object-based methods, but this is a cumbersome task for the purpose of this research since a large amount of models has to be generated. FLUMY® has been chosen to generate fluvial input models, as it is able to fulfill most of the requirements stated above.

2.1.1 FLUMY® Fluvial Systems

FLUMY® is a process-based and stochastic modeling tool. It models both meandering channel systems and turbidites at the scale of a reservoir. The Fluvial System Modeling tool is a based on the temporal evolution of a channel by migration, cut-off and avulsion. It models the related deposition of point-bars, mud-plugs, crevasse splays, overbank alluvium and organic matter (Figure 2.1).
The domain is discretized as a rectangular two dimensional grid. The domain has a deepening reference plane with a given global slope. The general flow direction is parallel to the plane dip direction. Time is discretized into time steps (iterations) and at every time step

migration of the channel is performed. The main parameter for the migration of the channel is erodability that can be either a constant value over the domain or defined as a map or matrix on the discretized grid.
During overbank flow, alluvium is deposited with grain size and thickness decreasing exponentially perpendicular to flow direction of the channel. Aggradation or incision may be constrained by the distance between the profile of the elevation of the domain and an equilibrium profile parallel to the reference plane. The equilibrium profile can vary in time.
At some time, a levee breach (either during overbank flow or random) can occur inside or outside the domain. This breach produces a chute cut-off or a crevasse splay. This crevasse splay can evolve into a local avulsion. In addition to the local avulsions, regional avulsions can occur caused by an levee breach further upstream that shifts the channels entry point in the domain. Abandoned channels are filled with a mud plug (FLUMY®, 2017).

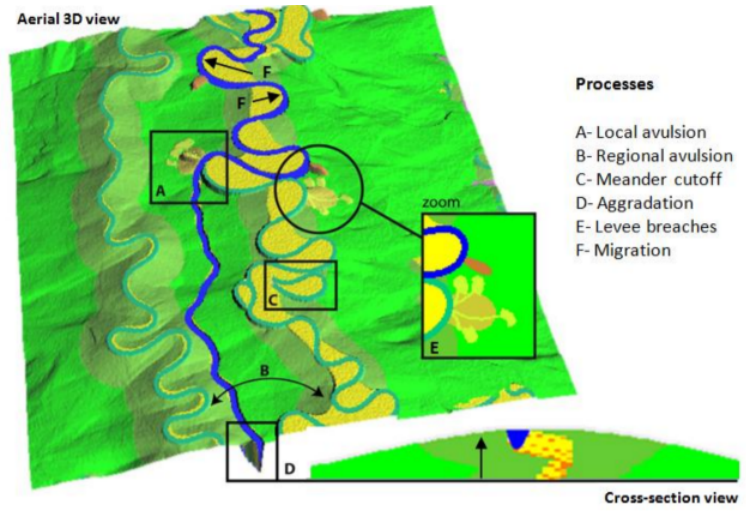

Process	Facies	Litho-facies	
Migration	Point bar	Sand	PB
	Channel lag	Gravel	CL
Cutoff	Abandoned meander (plug and loop)	Sand	SP
		Shale	MP
Aggradation	Levees	Silt	LV
	Overbank flood	Shale	OB
		Wetland	WL
Levee breaches	Crevasse splay 1	Sand	CS1
	Crevasse splay 2	Silt	CS2
	Crevasse channels	Sand	CCH
Avulsion	Abandoned channel	Sand	SP
		Shale	MP
	Channel Fill	Shale	CF
Marine incursion	Draping	Shale	DR

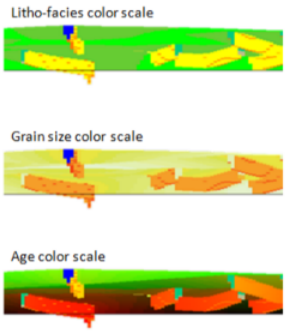

Figure 2.1: FLUMY output and processes related to the deposition of different litho-facies (FLUMY® (2017)).

2.1.2 FLUMY® Model Settings

FLUMY® enables the user to set a large variety of parameters in order to produce a model. This is very usefull in a case study, because it enables the user to generate a large variety of models. This study is a feasibility study and its main purpose is to compare the statistics

of the models based on well definable properties of a reservoir like net-to-gross and the geometry of the elements in the reservoir. FLUMY® has a built-in interface that provides the user the opportunity to generate a model that meets predefined reservoir characteristics. The inputs are a maximum channel depth, Sandbodies Extension Index (SEI[1]) and Net-to-Gross[2]. Figure 2.2 shows how the parameters affect the distribution of the sandstone bodies in the sample space.

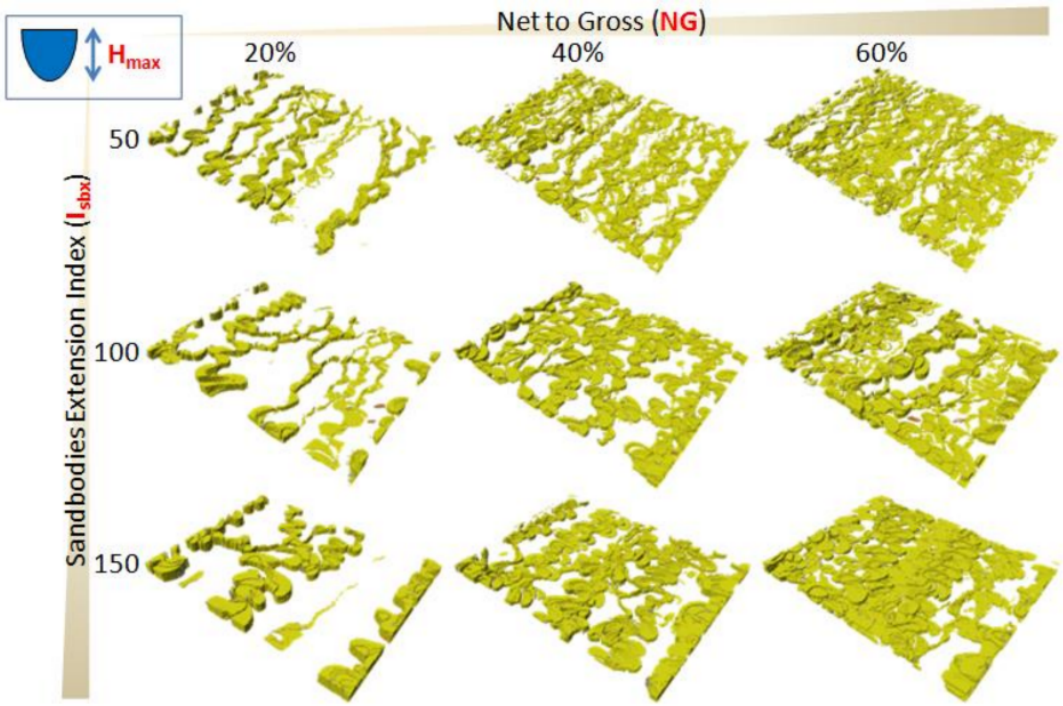

Figure 2.2: FLUMY® preliminary parameter settings and their effect on sandbody distribution and geometry in the reservoir FLUMY® (2017).

2.1.3 FLUMY® Outputs

The output of the simulation in FLUMY® is a successive deposition with a variable height on a two dimensional grid, depending on the height of the topography at the node, of the age, litho-facies and grain size. The final topography causes the output to be of irregular size in the vertical direction. The two dimensional grid with deposition units can be exported to a three dimensional grid format done by discretization. The resulting output is a three dimensional Cartesian grid of the age, litho-facies and grain size. The exported model is used as the input sample space for the REV evaluation.

1 The Sandbodies Extension Index (SEI) is a measure for the shape of a sandbody. A low SEI results in ribbon shaped sandstone bodies and a high SEI results in sheet like sandstone bodies.

2 The Net-to-Gross is a measure for the volume percentage of the reservoir where fluids can flow. For fluvial reservoirs, this comes more or less down to the volume percentage of the reservoir that is occupied by sandstone bodies

2.1.4 FLUMY® Output Models and the Assignment of Properties

The discretized FLUMY® Cartesian grid is exported with 500 x 500 x 300 (x, y, z) cells resulting in 75 million grid cells. The grid blocks are sized 10m x 10m x 0.5m (dx, dy, dz) (Figure 2.3). The resulting grid size is 5000m x 5000m x 300m (x, y, z) and has a volume of 3.75 cubic kilometer. The discretized grid is imported in MATLAB® and will be referred to as the sample space. All models have the same grid block size and sample space.

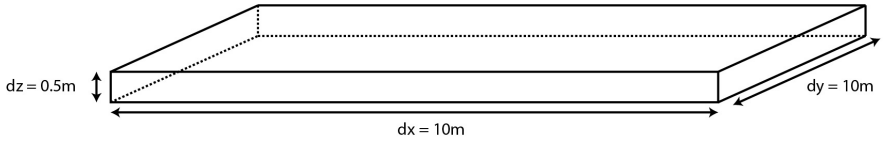

Figure 2.3: Grid cell size of the discretized FLUMY® output.

The models are populated with petrophysical properties based on the discretized grainsize assigned to the grid cell. FLUMY® assigns a grain size and a lithology to every cell. Figure 2.4 shows the lithologies and the associated grain sizes. The porosity and permeability are assigned to the grain sizes based on an educated guess. They do not represent any real world data. The porosity value is the effective porosity (i.e., the part of the porosity that could potentially contribute to flow) and is assigned such that it potentially could meet real world data. The permeability values are defined based on a cut-off value. Those grain sizes that would very likely contribute to flow are assigned 1000 mD whilst the grain sizes that very likely do not contribute to flow are assigned 1 mD. This means that we only consider the effect of geometry. All measurements will be relative to the upper and lower bound of the permeability. Introduction of more realistic permeability will likely increase the volume needed to be representative for the permeability (Norris and Lewis, 1991).

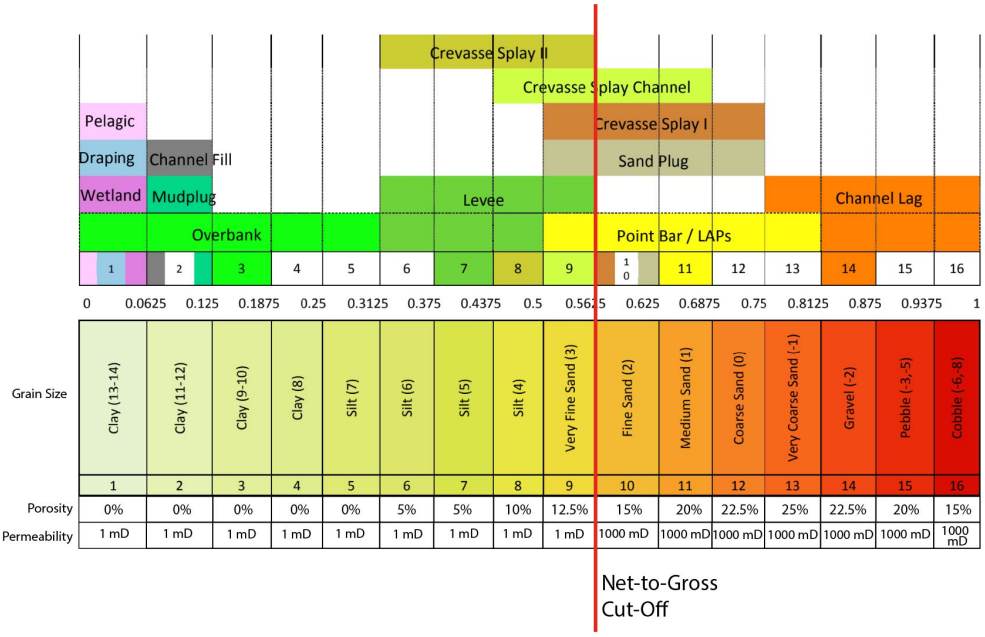

Figure 2.4: FLUMY® lithology output and associated grain size. The last two rows show the assigned petrophysical properties.

The clear cut-off has been used, because the main factor that affects the large scale flow through fluvial reservoirs is the large contrast between low permeable and high permeable deposits. This representation avoids assigning a specific value to the deposits, which highly differs per reservoir, but rather sees it as a relative difference between high and low permeable zones (i.e., only sandstone bodies significantly contribute to flow). A total of 21 models is generated. The maximum channel depth is kept constant. The Sandbody Extension Index (SEI) is set to 50, 80 and 110. For every SEI number, 8 models with varying expected Net-to-Gross are generated. After generation of the models in FLUMY®, the cells are populated with the properties from Figure 2.4. The expected Net-to-Gross is not equal to the Net-to-Gross of the populated grid, due to differences in cut-off values and FLUMY's inability to generate an expected Net-to-Gross explicitly. Table 2.1 shows the Net-to-Gross based on the Cut-Off defined in Figure 2.4.

	SEI = 50	SEI = 80	SEI = 110
NG = 5	8%	9%	9%
NG = 10	13%	15%	15%
NG = 15	18%	20%	22%
NG = 20	24%	25%	27%
NG = 30	33%	36%	38%
NG = 50	52%	55%	58%
NG = 70	69%	72%	75%

Table 2.1: Sample space Net-to-Gross values based on the Cut-Off values in Figure 2.4. The upper row shows the Sandbodies Extension Index (SEI) and the left column shows the expected Net-to-Gross.

2.2 EVALUATION OF FLUMY®MODELS AS A FUNCTION OF SAMPLE VOLUME

To be able to find a REV for fluvial models, the effect of sample volume on porosity and permeability has to be evaluated. This is done by sampling blocks with predefined size at random locations from the entire sample space. It is important to note that the sampling volume must be small with respect to the sampling space (i.e. ($V_{sample\,volume} << V_{sample\,space\,volume}$) and ($L_{sample\,length\,in\,x,y\,or\,z} << L_{sample\,space\,length\,in\,x,y\,or\,z}$)). Otherwise it would always converge to the property of the entire sample space, no matter the amount of heterogeneity (Sahimi and Islam, 1996).

2.2.1 Sub-Sample Number and Volume

The blocks are sampled from the sample space in a systematic manner. Every sampled block has the same amount of cells in x, y and z direction. This means that a block with sub-sample number 100 has 100 x 100 x 100 cells and has dimensions 1000m x 1000m x 50m with a total volume of $50x10^6\,m^3$. Figure 2.5 shows the relation between the sub-sample number and the volume of the cell. Figure 2.6 shows an example of five randomly sampled blocks with sub-sample numbers 20, 40, 60, 80 and 100. The yellow blocks represent the high permeable zones (sandstone bodies) and the blue blocks represent the low permeable zones (overbank deposits).

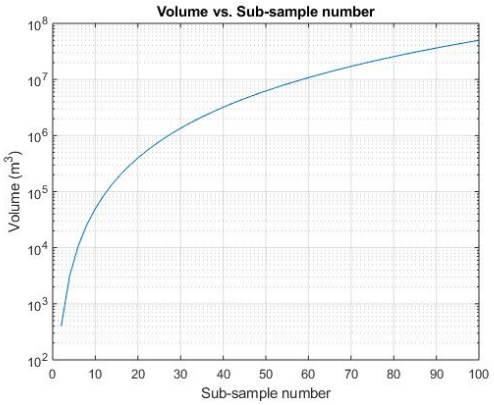

Figure 2.5: Sub-sample number versus block volume. The block volume is plotted at a logarithmic scale.

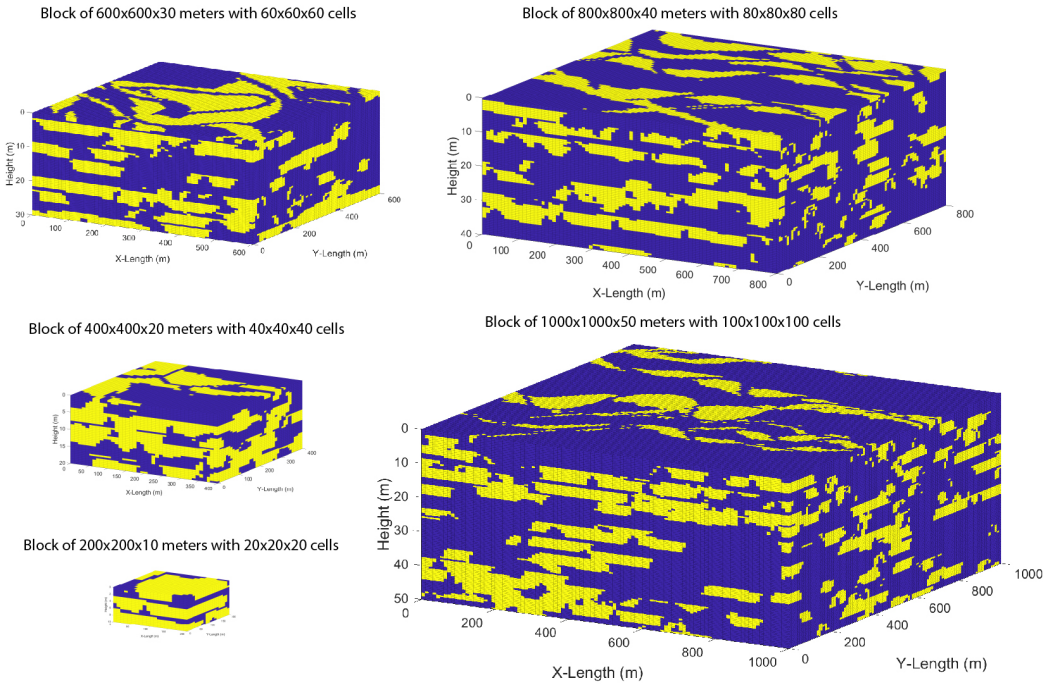

Figure 2.6: Five sampled blocks with sub-sample number 20, 40, 60, 80 and 100. The sub-sample number corresponds with a block with an equal amount of cells in three dimensions. Sub-sample number 100 has 100 x 100 x 100 cells and has dimensions 1000m x 1000m x 50m with a total volume of $50x10^6\ m^3$.

2.2.2 Sub-sampling Porosity

The sub-samples of porosity are sized between sub-sample number 2 ($400\ m^3$) and sub-sample number 100 ($50x10^6\ m^3$). A set of 1000 sub-samples from random locations in the sample size is taken for every even sub-sample number (2,4,6,8,...,100).

2.2.3 Sub-sampling Permeability

The sub-samples for permeability are sized between sub-sample number 2 ($400\,m^3$) and sub-sample number 100 ($50x10^6\,m^3$). A set of 100 sub-samples from random locations in the sample space is taken for every even (2,4,6,8,...,50) sub-sample number from 2 to 50. From sub-sample 55 to 100, a set of 20 sub-samples from random locations in the sample space is taken for every sub-sample number that is multiple of 5 (55,60,65,70,...,100). Table 2.2 shows the properties of the sample sizes schematically.

Property	Porosity	Permeability
Min sub-sample nr.	2	2
Max sub-sample nr.	100	100
Min Volume	$400\,m^3$	$400\,m^3$
Max Volume	$50x10^6\,m^3$	$50x10^6\,m^3$
Stepsize	2	2 from sub-sample number 2 to 50 5 from sub-sample number 50 to 100
Amount of samples per sub-sample volume	1000	100 until sub-sample number 50 20 from sub-sample number 50 to 100

Table 2.2: Sample size properties for porosity and permeability.

2.3 UPSCALING

In order to upscale the cells for the main reservoir properties, porosity and permeability, upscaling functions have to be used. It is important to note that the upscaling method is heavily dependent on the upscaled property. Generally, we can distinguish two property groups: Additive and non-additive properties. Additive properties, such as porosity, can be upscaled with simple averaging methods. Porosity is upscaled with simple arithmetic averaging. Non-additive properties, such as permeability, may be upscaled with simple averaging methods[3], but will often not give realistic results with more complex geometries and anisotropy (Bear, 1972; Desbarats, 1987; Durlofsky, 1991; Wen and Gómez-Hernández, 1996). Therefore, they are upscaled with numerical upscaling methods.

2.3.1 Porosity

The porosity, a function that inevitably arises from the *Continuum Approach*, is simply the ratio between the void space and the total sample volume (Equation 2.1).

$$\phi = \frac{V_{voids}}{V_{voids} + V_{matrix}} \tag{2.1}$$

Porosity is upscaled using weighted arithmetic averaging. Each factor is weighted by its volume, but since all cell sizes are equal, this reduces to the simple arithmetic average. Equa-

3 Simple upscaling methods include the arithmetic, harmonic and geometric mean. For 1D flow, the upscaled grid block permeability is perfectly represented by the harmonic mean of the permeabilities of the grid blocks (Wen and Gómez-Hernández, 1996). For 2D and 3D flow, the geometric mean of the upscaled grid block permeability will only yield a representative effective permeability value if the grid blocks have nearly random heterogeneity and local isotropy (Matheron, 1967; Durlofsky, 1991). In cases with almost perfect layering, harmonic-arithmetic or arithmetic-harmonic averaging can give proper results (Durlofsky, 1991).

tion 2.2 shows the formula for the weighted arithmetic average and its reduction the the simple arithmetic average.

$$\bar{\phi} = \frac{\sum_{i=1}^{n}(\phi_i * V_i)}{\sum_{i=1}^{n} V_i} \quad \rightarrow \quad \bar{x} = \frac{1}{n}\sum_{i=1}^{n}(\phi_i) \tag{2.2}$$

With $\bar{x}$ = Arithmetic mean, n = number of cells, ϕ_i = Cell property value and V_i = Cell volume.

2.3.2 Permeability

Permeability is a measure of the ability of a porous medium to allow fluids to pass through it. Permeability is mainly related to the porosity, geometry of the pores and the level of connectedness of a medium. It is often too complex to encompass all factors that affect flow through a porous medium. Therefore permeability is a widespread used parameter to circumvent modelling of flow of fluids through the matrix itself, but rather capture the void space and matrix as a continuum. Henry Darcy (1856) found that the flow velocity through a porous medium is proportional to the change of hydraulic head divided by the length of the sample. The change of hydraulic head over the length of the sample can be expressed as the rate of change of pressure vector (∇p). If we include the viscosity in the equation, Equation 2.3 shows the equation for the absolute permeability related to the superficial fluid flow. It is important to note that the *continuum approach* regarding permeability is only valid if the inertial forces are negligible as compared with that arising from viscosity (Laminar flow) (Hubbert, 1956). This is very often the case for flow of fluids through natural rocks.

$$q = -\frac{k}{\mu} \cdot \nabla p \tag{2.3}$$

With q = Superficial fluid flow velocity (m/s), k = Absolute permeability (m^2), μ = Viscosity of the fluid ($Pa \cdot m$) and ∇p = Pressure gradient vector (Pa/m).

Permeability can be upscaled with flow based upscaling methods. Multiple flow based upscaling methods exist. They can generally be divided into two groups: local and non-local upscaling methods. Local upscaling methods derive the effective permeability explicitly from the cell permeabilities within the upscaled block. However, the effective permeability can be heavily dependent on the boundary conditions applied to the block. This implies that block permeability is non-local (i.e. the effective permeability is not only a function of the cells within the upscaled block, but also a function of the flow conditions within the block that depend on boundary conditions applied to the block) (Wen and Gómez-Hernández, 1996). Therefore, non-local upscaling methods have been developed. These methods extend the domain of the computational boundary from the upscaled block. This reduces the dependency of effective permeability on the initial boundary conditions on the flow cell. Figure 2.7 shows an example of the extension of the flow domain in order to compute the effective permeability of the upscaled block. Wen and Gómez-Hernández (1996) and Durlofsky (2005) provide an extensive review of local and non-local upscaling methods. Indelman and Dagan (1993); Li et al. (1995); Durlofsky (1991); Holden and Nielsen (2000); Wen et al. (2003) are just a few of the papers concerning flow-based (non-local) upscaling techniques.

Single-Phase Flow-Based Permeability Upscaling with Sealed Sides Boundary conditions

This study uses single-phase flow-based permeability uspcaling with sealed sides boundary conditions. This method is proposed by Warren and Price (1961) and simulates a conventional

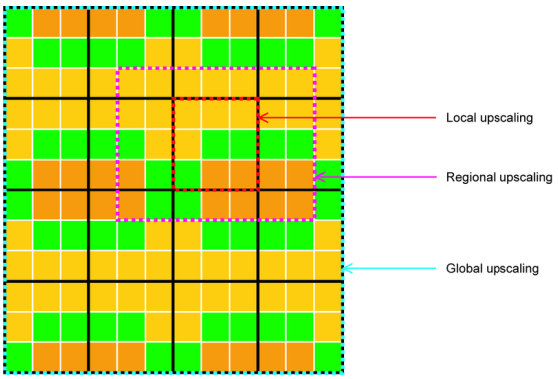

Figure 2.7: Local, regional and global upscaling methods (from PetroWiki (2015)).

core plug measurement, where two opposite sides are subjected to a pressure drop and all other sides are sealed. A conventional core plug is only examined in one direction, but a block can be subjected to three different directions with this method. Figure 2.8 shows a hypothetical block that is subjected to a pressure drop in three different directions.

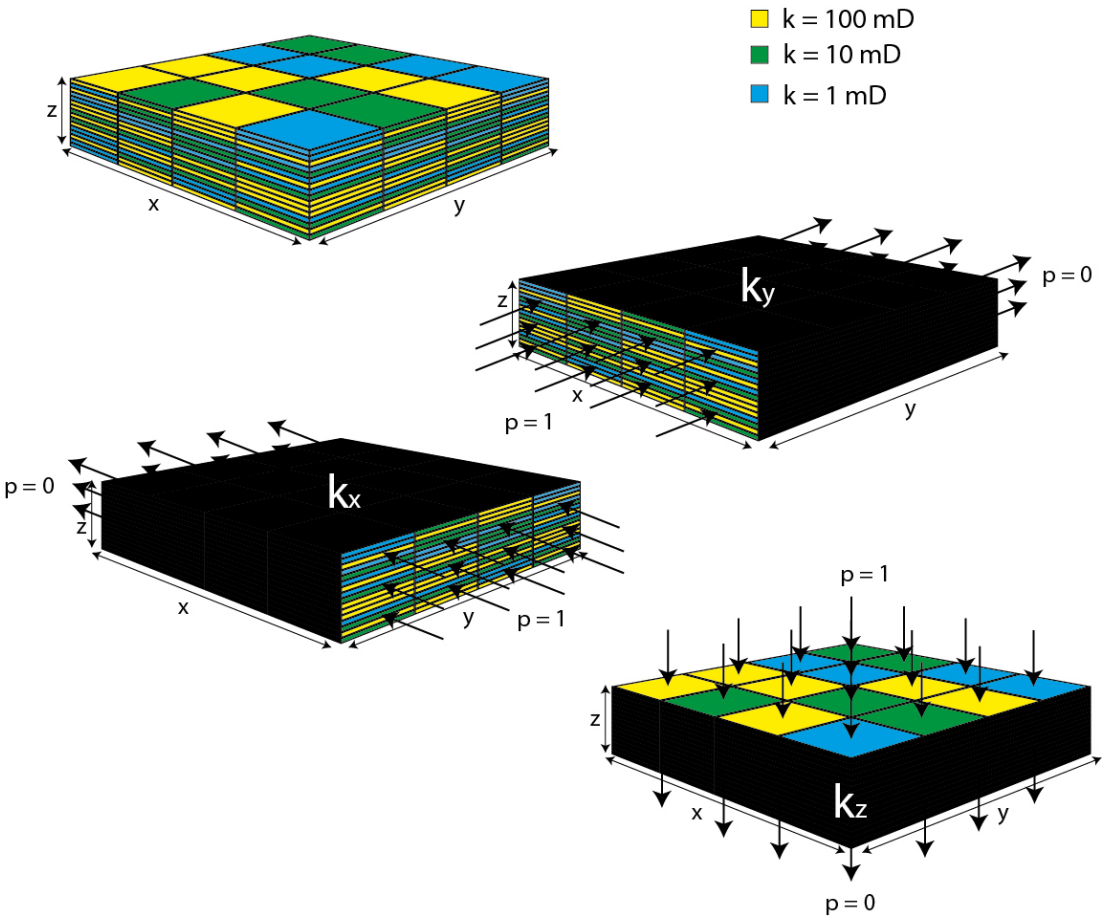

Figure 2.8: Flow-based 'scalar' permeability uspcaling with sealed sides boundary conditions (Warren and Price, 1961).

The permeability is determined with inverse Darcy's law by determining the outflow for a given input pressure difference. The upscaled block is assigned a three dimensional diagonal effective permeability tensor:

$$\underline{\underline{k_{eff}}} = \begin{bmatrix} k_x & 0 & 0 \\ 0 & k_y & 0 \\ 0 & 0 & k_z \end{bmatrix}$$

This method is the simplest, but also the most intuitive flow-based upscaling method (Durlofsky, 2005). This is one of the reasons this method is used in this study. Many other flow-based upscaling methods, such as local periodic, regional and global upscaling, provide a full three dimensional effective permeability tensor that is better able to capture the actual conditions imposed on the region during the course of flow simulation. Especially because the actual conditions imposed on the region are not known beforehand (Durlofsky, 2005). Still, although these arguments are valid in the strict sense of accurate upscaling, they are much more complex to simulate and process for the purpose of this research. A diagonal three dimensional effective permeability tensor is much easier to imagine and interpret. Moreover, the input models in this study are not sampled with random orientation. The general flow direction of all models is the same and the stacking pattern of the channels is not tilted with respect to the reference plane. The horizontal permeability in the x and y direction and the vertical permeability are therefore well aligned with the direction of the sandstone bodies. The main differences between the effective block permeability that is upscaled with single-phase flow-based upscaling with sealed sides boundary conditions and other single-phase flow-based upscaling methods will likely occur in small sub-samples. It is important to note that the single-phase flow-based permeability upscaling with sealed sides boundary conditions generally tends to underestimate the 'true' effective permeability (King and Mansfield, 1999). It thickens the barriers and narrows the flow paths. This effect decreases with increasing block size since a larger part of the sample space is sampled. A detailed description with formulas en governing equations of single-phase flow-based local upscaling with sealed sides boundary conditions can be found in: (Durlofsky, 2005, 11-12).

2.4 STATISTICAL ANALYSIS OF FLUVIAL DEPOSITIONAL SYSTEMS AS A FUNCTION OF SAMPLE VOLUME

The upscaled blocks with varying sample volume are analysed based on the statistical moments of the probability distribution that is computed for the sub-sample numbers in subsection 2.2.1. The set of sample properties for a certain sub-sample number is analysed based on the mean, standard deviation and coefficient of variation. Figure 2.9 shows a typical Box-Whisker plot of the probability distributions of the samples as a function of the sub-sample number. Every box (and whisker) represents one probability distribution. It is important to note that the mean of the probability distribution is the same for every sub-sample number for porosity (additive property). On the contrary, the mean of the probability distribution per sub-sample number could vary for permeability (non-additive property).

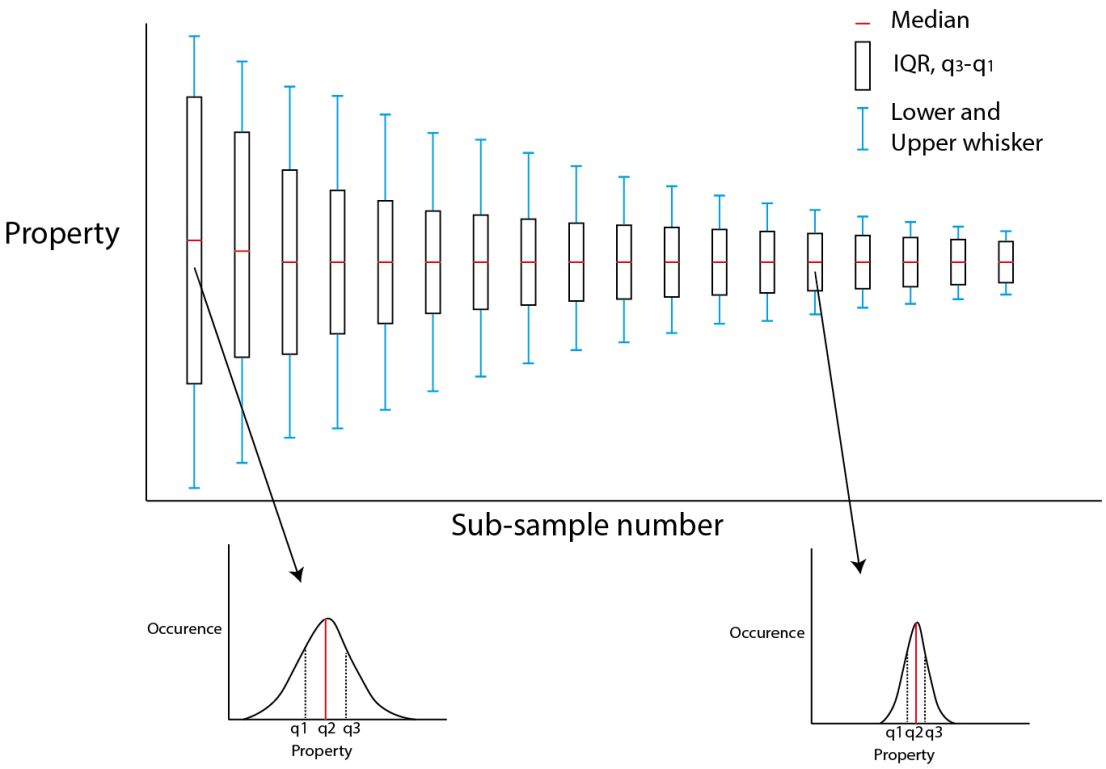

Figure 2.9: Typical Box-Whisker plot for a property as a function of the sub-sample number. Every box (and whisker) represents one probability distribution.

The set of property values per sub-sample number is analyzed based on the mean, standard deviation and coefficient of variation. The mean is the expected value of a probability distribution. The mean of the set of samples for a given sub-sample number is computed by Equation 2.4.

$$\mu = \frac{1}{n}\sum_{i=1}^{n}(x_i) \tag{2.4}$$

With μ = mean, n = number of samples and x_i = property value.

The standard deviation is a measure of the amount of variation or dispersion of a set of data values. For a normally distributed dataset, there is a chance of 68.2% that a property value is at maximum one standard deviation away form the mean. The standard deviation of the set of samples for a given sub-sample number is computed by Equation 2.5.

$$\sigma = \sqrt{\frac{1}{n}\sum_{i=1}^{n}(x_i - \mu)^2} \quad with \quad \mu = Equation\ 2.4 \tag{2.5}$$

With σ = standard deviation, n = number of samples, x_i = property value and μ = mean.

Permeability values may span several orders of magnitude and the standard deviation usually increases as the mean increases. The coefficient of variation is therefore a better estimator of the dispersion of a set of permeability values. The coefficient of variation can

be seen as a normalization of the standard deviation (i.e., it estimates the relative dispersion rather than the absolute dispersion of a dataset). The coefficient of variation of the set of samples for a given sub-sample number is computed by Equation 2.6.

$$C_v = \frac{\sigma}{\mu} \quad with \quad \mu = Equation\ 2.4 \quad and \quad \sigma = Equation\ 2.5 \tag{2.6}$$

With C_v = coefficient of variation.

Corbett and Jensen (1992) provide an extensive review of the use of the coefficient of variation for permeability measurements. They conclude that the coefficient of variation is representative for a set of samples if:

$$n_0 = 100C_v^2 \tag{2.7}$$

With n_o = the number of samples and C_v = coefficient of variation.

This criterion is not always met in case of the permeability measurements due to computational limitations. This makes the coefficient of variation curves less smooth, but since they are evaluated for multiple sub-sample numbers, a trend can be distinguished. This will further be discussed in the conclusions and discussions.

3 RESULTS

The aim of the research is to evaluate if it is possible to define a Representative Elementary Volume (REV) for fluvial depositional models. This is done by plotting the statistical moments of the probability functions as a function of sub-sample number. Figure 3.1 shows an example of the representation of the mean and standard deviation of the horizontal permeability parallel to the paleo-flow direction as a function of sub-sample volume for one specific model. The coefficient of variation is used as the measure of dispersion of the dataset. Theoretically, REV is reached when the coefficient of variation is zero and the mean does not vary with sample size. This criterion will not yield when the sample scale is small with respect to the scale of the heterogeneity. Consequently, a criterion has to be used that is robust and justifiable for the purpose of modeling. Therefore, the models are analyzed based on the curves for the mean, standard deviation and coefficient of variation without making statements about the REV beforehand. The discussion contains several methods to determine an REV and the criteria that can be used to define an REV.

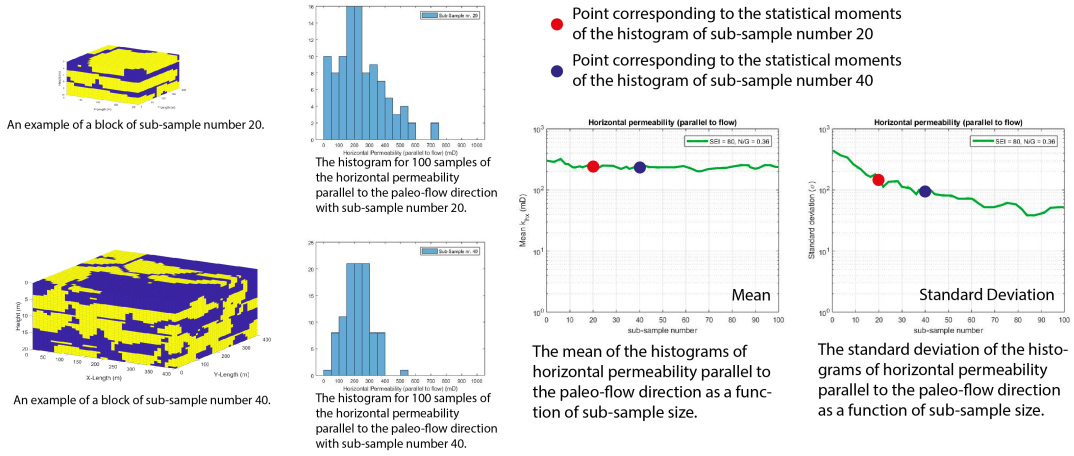

Figure 3.1: An example of the mean and standard deviation of the permeability parallel to the paleo-flow direction as a function of sample volume. The blocks are examples of a randomly sampled block. The histograms show the distribution for horizontal permeability parallel to the paleo-flow direction for 100 blocks sampled at size 20 and 40 respectively.

3.1 POROSITY AS A FUNCTION OF SAMPLE VOLUME

The mean, standard deviation and coefficient of variation of porosity are plotted as a function of sample volume. Since porosity is an additive value, the mean of the porosity should not vary with sample volume. The sampling of the porosity serves both as a proof of concept for the model and as a method for comparison with the permeability as a function of sample volume. Permeability is much more difficult to analyse, especially because the mean can vary. The analysis of the porosity can therefore serve an important role as a model check and a comparison for the analysis of the permeability.

3.1.1 Mean as a Function of Sample Volume

The mean of the porosity as a function of sample volume for a Sandbodies Extension Index of 50, 80 and 110 with multiple Net-to-Gross ratios is plotted in Figure 3.2a, Figure 3.2b and Figure 3.2c respectively. Although the sample spaces with low Net-to Gross show variation in the mean for smaller sub-samples, there is no clear trend of increase or decrease of the mean as a function of sample volume.

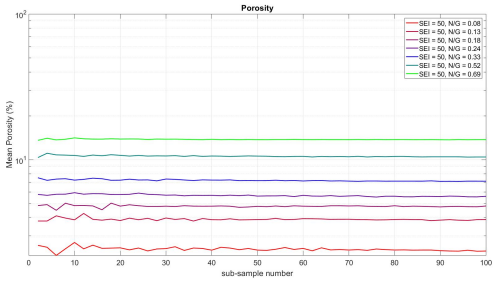

(a) The mean of the porosity as a function of sample volume for models with a Sandbodies Extension Index of: 50.

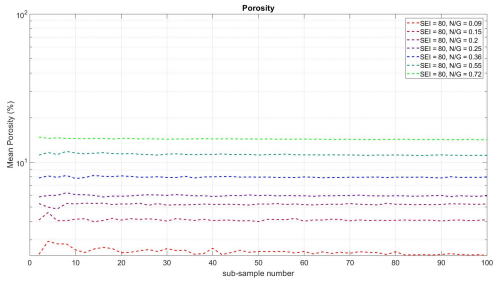

(b) The mean of the porosity as a function of sample volume for models with a Sandbodies Extension Index of: 80.

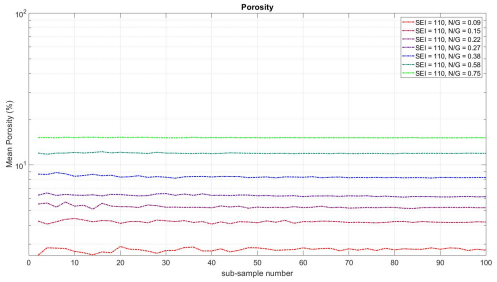

(c) The mean of the porosity as a function of sample volume for models with a Sandbodies Extension Index of: 110.

Figure 3.2: The mean of the porosity as a function of sample volume.

3.1.2 Standard Deviation as a Function of Sample Volume

The standard deviation of the porosity as a function of sample volume for a Sandbodies Extension Index of 50, 80 and 110 with multiple Net-to-Gross ratios is plotted in Figure 3.3a, Figure 3.3b and Figure 3.3c respectively. The standard deviation as a function of sample volume shows convergence towards lager sample volumes for all curves. It is clearly visible

that the standard deviation for the smallest sub-sample (2x2x2) is heavily dependent on the the Net-to-Gross ratio for all different models. All three models have the highest initial standard deviation for a Net-to-Gross between 0.33 and 0.58 and the lowest initial standard deviation for a Net-to-Gross between 0.08 and 0.09. The highest Net-to-Gross curve (between 0.69 and 0.75, depending on the model) converges significantly faster than the curves for lower Net-to-Gross.

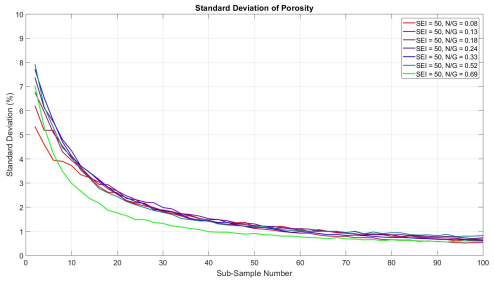

(a) The standard deviation of the porosity as a function of sample volume for models with a Sandbodies Extension Index of: 50.

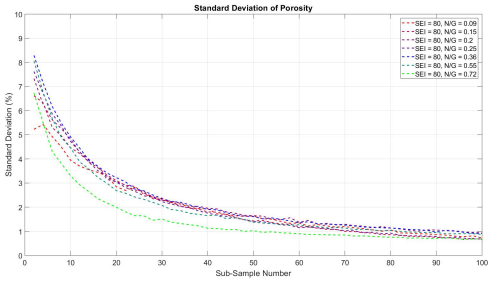

(b) The standard deviation of the porosity as a function of sample volume for models with a Sandbodies Extension Index of: 80.

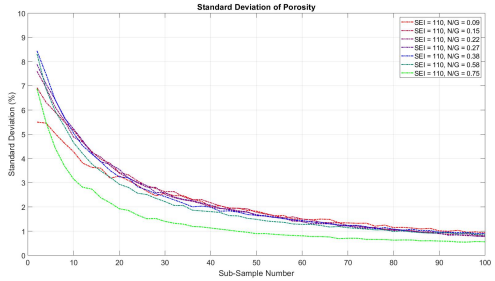

(c) The standard deviation of the porosity as a function of sample volume for models with a Sandbodies Extension Index of: 110.

Figure 3.3: The standard deviation of the porosity as a function of sample volume.

3.1.3 Coefficient of Variation as a Function of Sample Volume

The Coefficient of Variation of the porosity as a function of sample volume for a Sandbodies Extension Index of 50, 80 and 110 with multiple Net-to-Gross ratios is plotted in Figure 3.4a, Figure 3.4b and Figure 3.4c respectively. All curves show a logarithmic decline. It is clearly visible that the coefficient of variation is heavily dependent on the Net-to-Gross ratio. This is fairly intuitive considering the standard deviation curves that are fairly similar to each other except for the Net-to-Gross ratios above 0.69. It is important to observe that the some curves in Figure 3.4a and Figure 3.4b show a more rapid decline of the coefficient of variation after sub-sample number 60. For sub-sample numbers higher than 60, this results in a higher coefficient of variation for models with a higher Net-to-Gross ratio than models with a smaller Net-to Gross ratio. This deviates from the general trend that the coefficient of variation is higher for models with a low Net-to-Gross ratio.

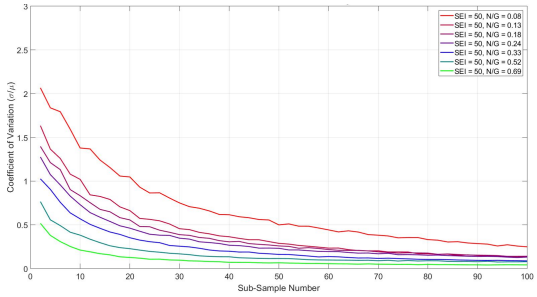

(a) The coefficient of variation of the porosity as a function of sample volume for models with a Sandbodies Extension Index of: 50.

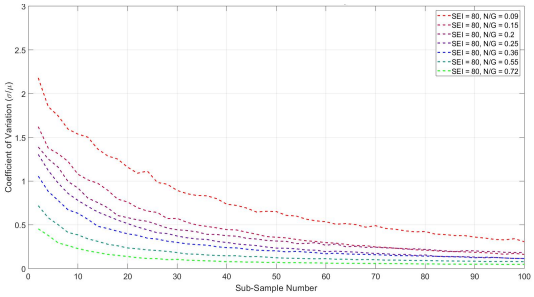

(b) The coefficient of variation of the porosity as a function of sample volume for models with a Sandbodies Extension Index of: 80.

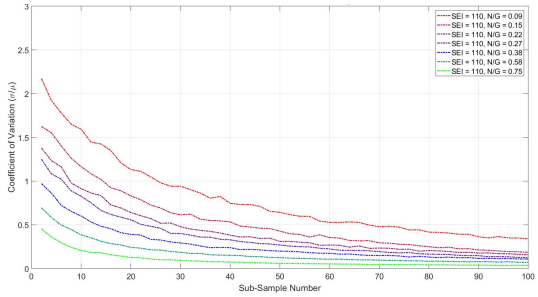

(c) The coefficient of variation of the porosity as a function of sample volume for models with a Sandbodies Extension Index of: 110.

Figure 3.4: The coefficient of variation of the porosity as a function of sample volume.

3.2 PERMEABILITY AS A FUNCTION OF SAMPLE VOLUME

The mean, standard deviation and coefficient of variation of the two horizontal and the vertical permeability are plotted as a function of sample volume. Since permeability is an non-additive value, the mean of the permeability may vary with sample volume, to the contrary of porosity, where the mean does not vary with sample volume. This section only shows the curves for a Sandbodies Extension Index of 50, because the directional effective permeability tensor gives three permeability curves resulting in a large amount of data. The curves for the mean, standard deviation and coefficient of variation of the different Sandbodies Extension Index show similar behavior. The curves for all models are visualized in Appendix B.

3.2.1 Mean as a Function of Sample Volume

The mean of the horizontal permeability parallel to the paleo-flow direction, horizontal permeability perpendicular to the paleo-flow direction and vertical permeability as a function of sample volume for a Sandbodies Extension Index of 50 with multiple Net-to-Gross ratios is plotted in Figure 3.5a, Figure 3.5b and Figure 3.5c respectively. The mean of the permeability as a function of sample volume for all models is plotted in Appendix B. A clear trend is visible for both horizontal permeability and vertical permeability. The mean for all permeabilities is highest for high Net-to-Gross and lowest for low Net-to-Gross. The decrease of the mean as a function of sample volume is much more drastic for the vertaical permeability than for both horizontal permeabilities. All curves show a decrease of the mean with an increase of sample volume. The mean of low Net-to-Gross sub-samples tends to converge at a larger sub-sample size than high Net-to-Gross samples for the both horizontal permeabilities. On the contrary, the mean of high Net-to-Gross sub-samples tends to converge at a larger sub-sample size than low Net-to-Gross samples for the vertical permeability.

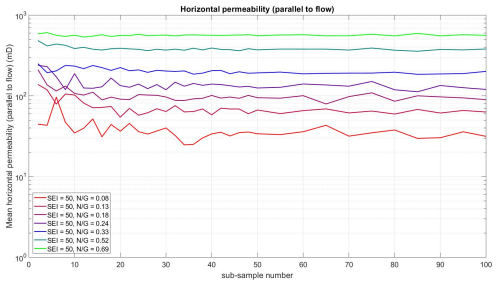

(a) The mean of the horizontal permeability parallel to the paleo-flow direction.

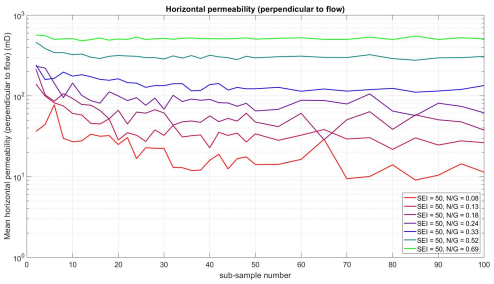

(b) The mean of the horizontal permeability perpendicular to the paleo-flow direction.

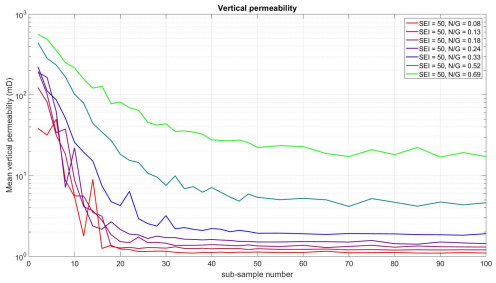

(c) The mean of the vertical permeability.

Figure 3.5: The mean of the permeability as a function of sample volume for models with a Sandbodies Extension Index of: 50.

3.2.2 Standard Deviation as a Function of Sample Volume

The standard deviation of the horizontal permeability parallel to the paleo-flow direction, horizontal permeability perpendicular to the paleo-flow direction and vertical permeability as a function of sample volume for a Sandbodies Extension Index of 50 with multiple Net-to-Gross ratios is plotted in Figure 3.6a, Figure 3.6b and Figure 3.6c respectively. The standard deviation of the permeability as a function of sample volume for all models is plotted in Appendix B. The standard deviation of the permeability in all directions shows a decline as a function of sub-sample size, but tends to be more dependent on Net-to-Gross ratio than the porosity. The difference is more distinct for the vertical permeability than for the horizontal permeability. Another difference between the standard deviation of horizontal permeability and the vertical permeability is the relative decline of standard deviation for different Net-to-Gross ratios. The standard deviation of vertical permeability shows the fastest decline for the lowest Net-to-Gross ratio and the slowest decline for the highest Net-to-Gross ratio. On the contrary, the standard deviation of horizontal permeability shows the fastest decline for the lowest Net-to-Gross ratio, but the slowest decline for the Net-to-Gross ratios between 0.3 and 0.6 depending on the sandstone body geometry of the model.

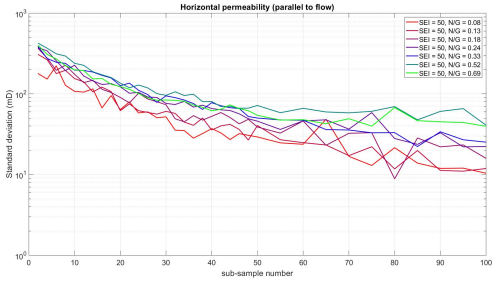

(a) The standard deviation of the horizontal permeability parallel to the paleo-flow direction.

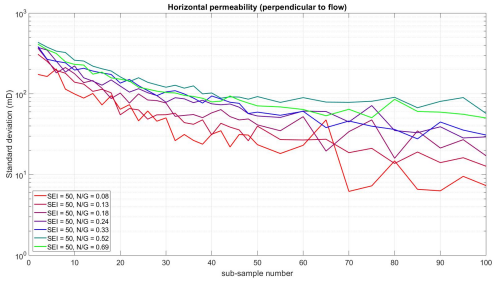

(b) The standard deviation of the horizontal permeability perpendicular to the paleo-flow direction.

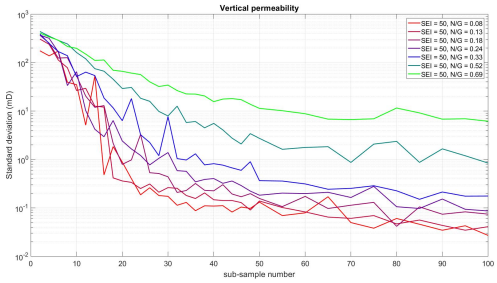

(c) The standard deviation of the vertical permeability.

Figure 3.6: The standard deviation of the permeability as a function of sample volume for models with a Sandbodies Extension Index of: 50.

3.2.3 Coefficient of Variation as a Function of Sample Volume

The coefficient of variation of the horizontal permeability parallel to the paleo-flow direction, horizontal permeability perpendicular to the paleo-flow direction and vertical permeability as a function of sample volume for a Sandbodies Extension Index of 50 with multiple Net-to-Gross ratios is plotted in Figure 3.7a, Figure 3.7b and Figure 3.7c respectively. The coefficient of variation of the permeability as a function of sample volume for all models is plotted

in Appendix B. The coefficient of variation of the horizontal permeability shows a general decline for all curves, with the coefficient of variation heavily dependent on the Net-to-Gross ratio. The coefficient of variation of the vertical permeability shows more peculiar behavior with an increase of the coefficient of variation after which it declines for all different curves. The peak of the coefficient of variation tends to be at a higher sub-sample size for higher Net-to-Gross ratios.

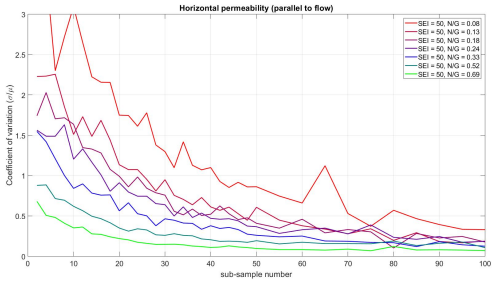

(a) The coefficient of variation of the horizontal permeability parallel to the paleo-flow direction.

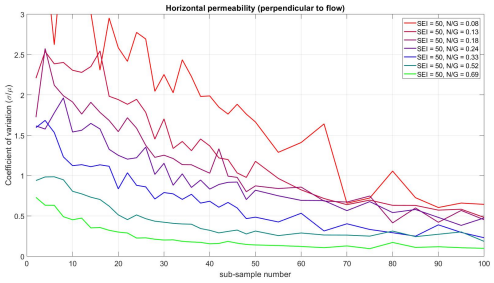

(b) The coefficient of variation of the horizontal permeability perpendicular to the paleo-flow direction.

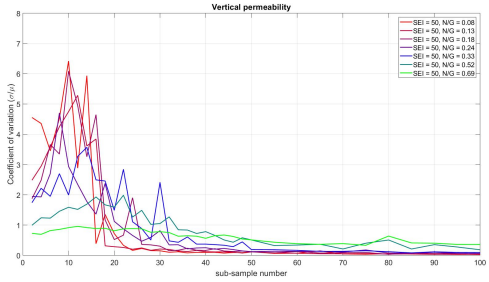

(c) The coefficient of variation of the vertical permeability.

Figure 3.7: The coefficient of variation of the permeability as a function of sample volume for models with a Sandbodies Extension Index of: 50.

4 DISCUSSION

This chapter will focus on the statistical moments of the permeability as a function of sample volume. The behavior of the curves of the statistical moments is translated to the input properties of the models. The behavior is explained with both mind experiments and cross-sections of the models. Furthermore, it will address the question if it might be possible to determine the 'true' effective permeability at REV scale without sampling at REV scale. The final part of this chapter discusses the possible applications of the results from this study.

4.1 SAMPLING AND PROBABILITY DISTRIBUTIONS

The evolution of probability distributions of effective properties as a function of sample size forms the most important part of this study. The probability distributions are analyzed based on their statistical moments, but these statistical moments tell little about the shape of the distribution. Figure 4.1 shows a very simple two layered high contrast permeability field. It is easy to imagine that the probability distribution of an infinitely small sub-sample at random locations from the sample space would either capture a high or a low permeability. If there is no initial difference in vertical and horizontal permeability, the distribution of the sub-samples is bi-modal and will yield for both vertical and horizontal permeability the same probability distribution. If the sub-sample size gets larger with respect to the scale of the geo-bodies, the chance of sampling both high and low permeability in one sub-sample increases. This is clearly visualized in Figure 4.1 where the lines indicate the part of the sample space where a sub-sample samples captures both high and low permeability values. The influence on the probability distribution of the horizontal and vertical permeability will be different. The horizontal permeability will go from a symmetric bi-modal probability distribution to a normal probability distribution and the expected value will be the same for all distributions, since it converges to the arithmetic mean of the entire sample space. The vertical permeability will go from a symmetric bi-modal probability distribution to a asymmetric bi-modal probability distribution and the expected value will decrease as a function of sample volume, since it converges to the harmonic mean of the entire sample space (Figure 4.1). The evolution of probability distributions as a function of sub-sample size and its relation with the sampled properties is important to keep in mind in order to get a better understanding of the influence of geometry on effective properties and REV. Most high permeability contrast sedimentary deposits show horizontal layering due to the nature of deposition. The harmonic and arithmetic mean of a perfect layered system generally form the upper and lower bounds of the 'true' effective permeability. This knowledge, in combination with the evolution of probability distributions as a function of sub-sample size forms the foundation of the evaluation of the effect of geometry on effective permeability as a function of sub-sample size and REV.

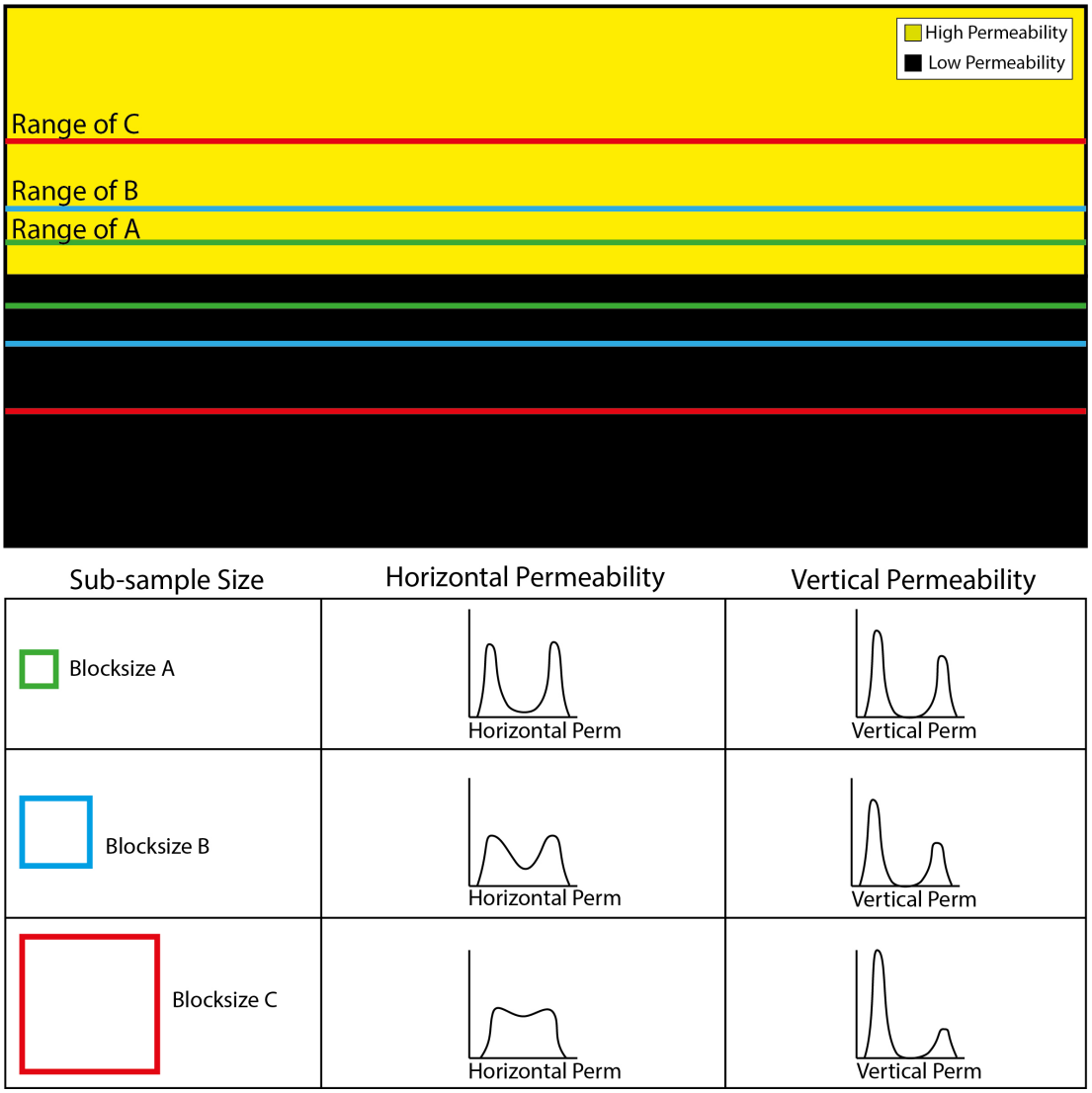

Figure 4.1: The upper figure shows a very simple two layered system with a high permeable and low permeable layer. The lines represent the range that for which a random sub-sample captures at least a part of the high and low permeable layer. It is easy to understand that if the sub-sample size is infinitely small, the probability distribution is bi-modal, it either captures a high permeable sample or a low permeable sample. If the sub-sample size increases, the likelihood of capturing both a part of the low permeable and the high permeable layer in one sample increases. This is why small sub-samples of high contrast permeability fields generally show a bi-modal distribution. As the size of the sub-sample increases, the probability distribution tends to be shaped more like a normal or log-normal distribution depending on the measured property. The graphs show hypothetical probability distributions as a function of sub-sample volume for both horizontal and vertical permeability. The horizontal permeability converges to a value that is the arithmetic mean of the entire sample space and the distribution tends to go from a symmetric bi-modal to a normally distributed probability distribution. The vertical permeability converges to a value that is the harmonic mean of the entire sample space and tends to go from a symmetric bi-modal to a asymmetric bi-modal distribution.

4.2 MEAN EFFECTIVE PERMEABILITY

The coefficient of variation and the standard deviation of permeability clearly do not converge to zero within the volume range that is sampled (Appendix B). Although many curves reach values that are within the threshold of a coefficient of variation of 0.5 that Corbett and Jensen (1992) define as a homogeneous, this threshold is disputable and heavily dependent on the purpose. The mean effective permeability curves show clear convergence for larger volumes. This indicates that, although the variation between the sub-samples is still large, the mean of the samples becomes (more) representative for the 'true' effective permeability at the scale of REV. Even more, it indicates that it could be unnecessary to capture the effective permeability at the REV scale (i.e., the scale where there is no variation between the samples), but rather capture its value where the mean does not change as a function of sample volume. Desbarats (1989); Deutsch (1989) have used this criterion for determining the statistical properties of flow in mud-sand systems. It must be noted that it is not known at which scale the effective property is not a function of sample volume any more (REV). Objections exist to this this assumption from which a couple are addressed in section 4.4 and section 4.5.

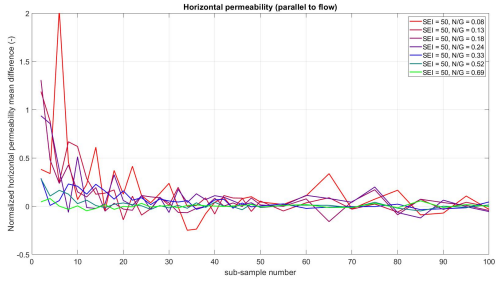

(a) The dimensionless mean difference between the horizontal permeability parallel to the paleo-flow direction and mean of the horizontal permeability parallel to the paleo-flow direction between sub-sample size 90 and 100 as a function of sample volume for samples with a Sandbodies Extension Index of 50.

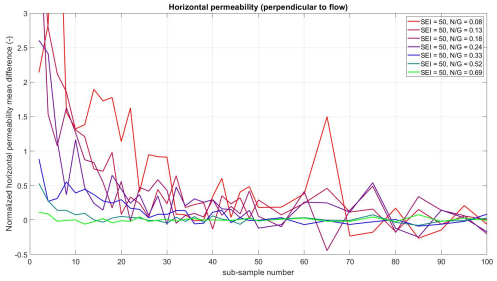

(b) The dimensionless mean difference between the horizontal permeability perpendicular to the paleo-flow direction and mean of the horizontal permeability perpendicular to the paleo-flow direction between sub-sample size 90 and 100 as a function of sample volume for samples with a Sandbodies Extension Index of 50.

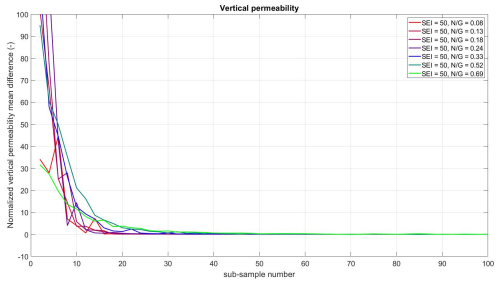

(c) The dimensionless mean difference between the vertical permeability and mean of the vertical permeability between sub-sample size 90 and 100 as a function of sample volume for samples with a Sandbodies Extension Index of 50.

Figure 4.2: The dimensionless mean difference between the permeability and mean of the permeability between sub-sample size 90 and 100 as a function of sample volume for samples with a Sandbodies Extension Index of 50.

4.2.1 Dimensionless Mean Difference of the Effective Permeability

The curves in Figure 4.2 show the dimensionless difference between the mean of the permeability of a sub-sample size and the mean of the permeability of sub-sample sizes 90 to 100 for models with a Sandbodies Extension Index of 50. The mean of the permeability of the sub-samples between 90 and 100 is chosen to diminish the variation caused by the low sample support at large sub-sample sizes (i.e., 20 samples per sub-sample size). More detailed curves for all models are plotted in Appendix C. If we assume that the mean of the permeability of sub-samples between 90 and 100 is representative for the 'true' effective permeability at the REV scale, we can plot the dimensionless difference between the mean of the permeability of a sub-sample size and the assumed 'true' effective permeability. The dimensionless difference is used to evaluate the convergence of the curves. The horizontal permeability parallel to paleo-flow for small sub-sample sizes can be two times higher than the horizontal permeability parallel to paleo-flow for low Net-to-Gross. The variation does not show a clear trend for sub-samples larger than 30 and variation is expected to be caused by the small amount of samples (i.e., 20 samples per sub-sample size after sub-sample size 50). The horizontal permeability perpendicular to paleo-flow for small sub-sample sizes can be more than three times higher than the horizontal permeability perpendicular to paleo-flow for low Net-to-Gross. The variation does not show a clear trend after sub-sample size 70 and variation is expected to be caused by the small amount of samples (i.e., 20 samples per sub-sample size after sub-sample size 50). The vertical permeability shows an even more drastic trend. The vertical permeability for small sub-sample sizes can be more than hundred times higher than the vertical permeability for low Net-to-Gross. The variation does not show a clear trend after sub-sample size 70.

4.2.2 The Mean Effective Permeability as a Function of Net-to-Gross

A curve of the effective permeability of fluvial positional system as a function of Net-to-Gross ratio can be plotted under the assumption that the mean of the permeability between sub-sample size 90 and 100 is representative for the 'true' effective permeability at REV (i.e., the sample size where there is no or little variation in the mean effective permeability between the sub-sample sizes). These curves can be compared with the curves for minimal (harmonic mean) and maximal (arithmetic mean) effective permeability values in a perfectly layered system. The geometric mean as a function of sample volume is plotted as a representation of a sample space with random heterogeneity and local anistropy. The curves for horizontal permeability (parallel and perpendicular to the paleo-flow direction) and vertical permeability with three different sandbody geometries as a function of Net-to-Gross are plotted in Figure 4.3.

4.2.3 Horizontal Permeability

Figure 4.3 shows that the expected value of the horizontal permeability parallel and perpendicular to flow diverge more from the arithmatic average if the Net-to-Gross decreases. The divergence from the arithmatic average is more drastic for the horizontal permeability perpendicular to flow than for the horizontal permeability parallel to flow. Even more, the ribbon type deposits tend to have a significantly lower effective permeability perpendicular to paleo-flow than the models with more sheetlike deposits. On the other hand does the effective permeability parallel to paleo-flow exhibit little difference between the different type of sandbody geometries. This difference is quite intuitive if we consider that a flow path (connectivity) is generally easier established in the paleo-flow direction of the river, if we assume that the point bars are connected (Donselaar and Overeem, 2008), than perpendicular to the

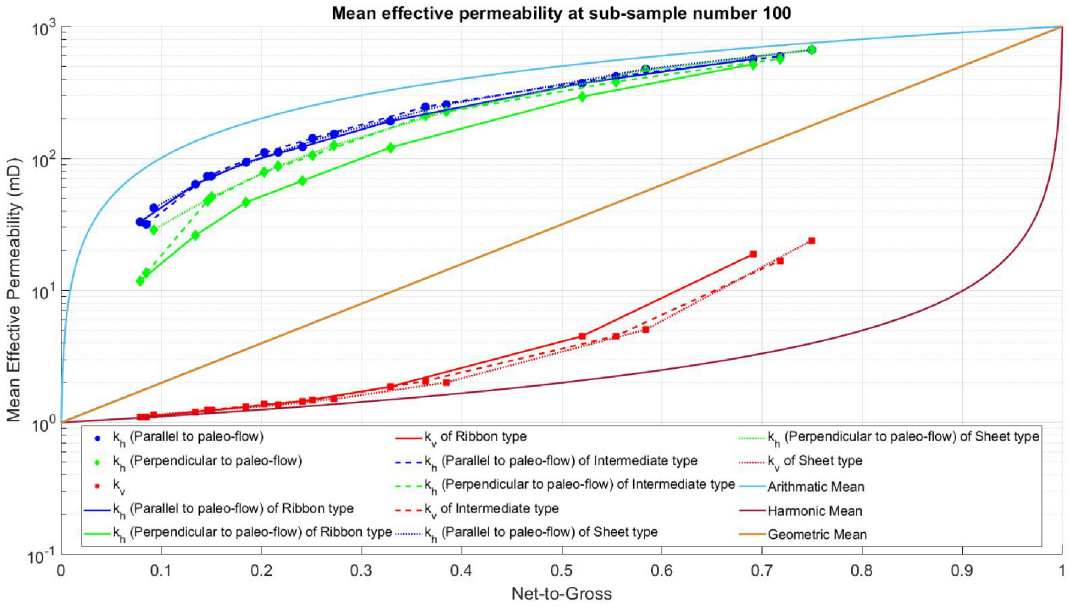

Figure 4.3: The mean of the effective permeability between sub-sample sizes 90 and 100. The three solid lines represent the harmonic, geometric and arithmetic mean for a Net-to-Gross ratio. For a perfectly layered medium, the effective vertical and horizontal permeability is represented by the harmonic and arithmetic mean respectively. The geometric mean represents the permeability for random heterogeneity and local anisotropy.

paleo-flow direction of the river, where the pointbars have to be connected by a process of incision and amalgamation. Even if the point bars are not connected by the sedimentary nature of the rives system, the likelihood of being connected is expected to be larger in the direction of the paleo-flow than perpendicular to it. The process of incision and amalgamation also forms a reason for the difference between the expected value of the effective permeability perpendicular to the paleo-flow direction of deposits that are sheetlike or ribbon type. A ribbon type sandbody is much less likely to connect with other sandstone bodies, because it exhibits less lateral width perpendicular to the flow direction. It is worth nothing that a river system that shows less trend in the general flow direction will be expected to show a more uniform horizontal permeability (i.e., the effective horizontal permeability in all directions shows less spread) an connectivity is expected to increase.

4.2.4 Vertical Permeability

Figure 4.3 shows that the expected value of the effective vertical permeability follows the line of the harmonic mean below a Net-to-Gross around 0.25. The expected value of the effective vertical permeability slowly diverges from the harmonic mean above a Net-to-Gross of 0.25. This behavior is strikes with conclusions about 3D-connectivity of fluvial depositions systems from Larue and Hovadik (2006); Pranter and Sommer (2011); Willems et al. (2017). They show that connectivity generally increases from very little to almost 100 % connectivity between Net-to-Gross ratios of 0.2 and 0.3.

4.3 REV, MEAN EFFECTIVE PERMEABILITY AND GEOMETRY IN FLUVIAL DEPOSITIONAL SYSTEMS

The main goal of this study is to evaluate if it is possible to translate the REV theorem to the scale of the fluvial depositional system. It is therefore valuable to translate the results of this study (i.e., the statistical moments of the probability distributions of porosity and permeability as a function of sample volume) back to the geological concepts that are distinctive for a fluvial depositional system. Cross-sections of models with different Net-to-Gross ratios and different sandstone body geometries are visualized in Figure 4.4 and Figure 4.7.

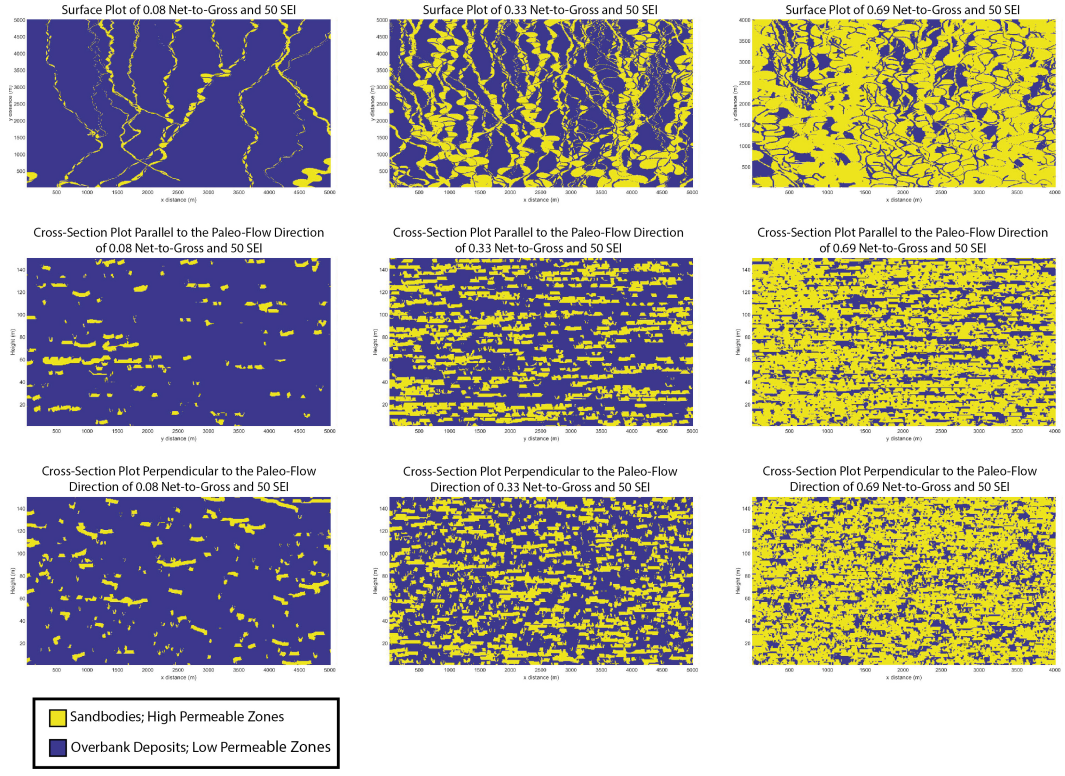

Figure 4.4: A comparison of three cross-sections from three models with a different Net-to-Gross ratio, but the same sandstone body geometry (SEI is 50). The left, middle and right three figures are cross-sections taken from a model with a Net-to-Gross ratio of 0.08, 0.33 and 0.69 respectively. The upper three figures are horizontal slices of the models, the middle three figures are vertical slices parallel to the paleo-flow direction and the lower three figures are vertical slices perpendicular to the paleo-flow direction.

4.3.1 REV, Mean Effective Permeability and Net-to-Gross Ratio

Figure 4.4 shows cross-sections in three dimensions of three different models with varying Net-to-Gross ratios and identical sandstone body geometries. All models have a Sandbodies Extension Index of 50 (ribbon type deposits) and a Net-to-Gross ratio from left to right of 0.08, 0.33 and 0.69. Figure 4.5 and Figure 4.6 show curves of the mean and coefficient of variation of the probability distributions of the effective permeability in three directions as a function of sample volume. Nine curves are plotted. The curves with the same line style have the same

Sandbodies Extension Index and the curves with the same color have a comparable Net-to-Gross ratio. Figure 4.5 and Figure 4.6 show that Net-to-Gross is the most important parameter for the values of the statistical moments of the probability distributions of the permeability as a function of sample volume. The behavior of the curves in Figure 4.5 and Figure 4.6 can be explained by a visual comparison of the cross-sections in Figure 4.4. This is done for three different directions, since the behavior of the statistical moments of permeability as a function of sample volume is heavily dependent on the orientation of the permeability with respect to the sandstone bodies.

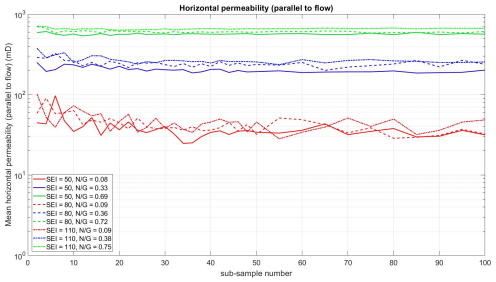

(a) The mean of the horizontal permeability parallel to the paleo-flow direction.

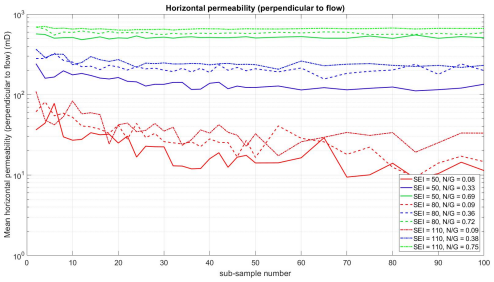

(b) The mean of the horizontal permeability perpendicular to the paleo-flow direction.

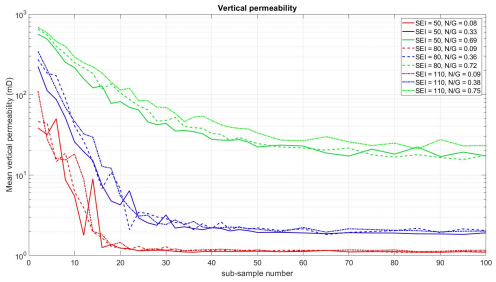

(c) The mean of the vertical permeability.

Figure 4.5: The mean of the permeability as a function of sample volume for models with a Sandbodies Extension Index of 50, 80 and 110 and comparable Net-to-Gross ratios.

Horizontal Permeability Parallel to the Paleo-Flow Direction

A low Net-to-Gross ratio results in sandstone bodies that are more or less independent flow paths within the clay matrix (overbank deposits). Therefore, the wavelength of the sandstone body is the main factor influencing the mean effective horizontal permeability parallel to the paleo-flow direction (i.e., the wavelength of the sandstone bodies is the dominant length scale). The mean of the effective horizontal permeability parallel to the paleo-flow direction will stay constant if a large enough part of the tortuous flow path is captured. The variability between the samples with a low Net-to-Gross ratio will be high compared to higher Net-to-Gross ratios, because there is a large chance of capturing parts of the model where there are no sandstone bodies (Figure 4.4). If the Net-to-Gross ratio increases, the sandstone bodies become more and more amalgamated. Therefore, the flow paths become less and less tortuous if we assume that the sandstone body geometry does not change. This can be compared with adding multiple sine waves with different offsets. If the waves are combined, the mean amplitude will be lower and lower if we increase the amount of waves with different offsets. This results in less tortuous flow paths and a lower dominant length scale (Figure 4.5a and Figure 4.6a). Another effect of increasing the Net-to-Gross ratio is the increase of the likelihood of capturing a sample that is representative for the model as a whole. This can be seen

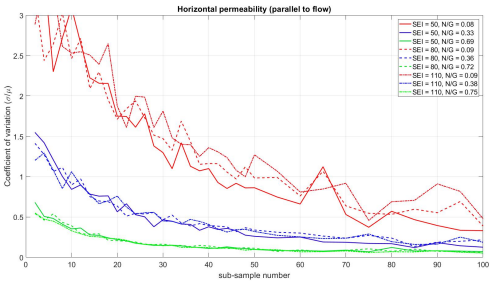

(a) The coefficient of variation of the horizontal permeability parallel to the paleo-flow direction.

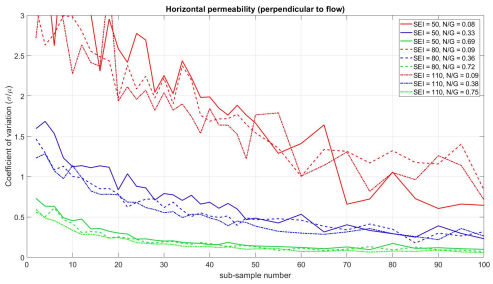

(b) The coefficient of variation of the horizontal permeability perpendicular to the paleo-flow direction.

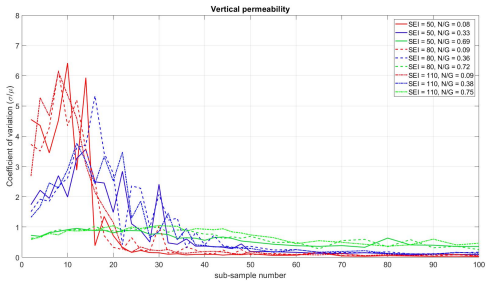

(c) The coefficient of variation of the vertical permeability.

Figure 4.6: The coefficient of variation of the permeability as a function of sample volume for models with a Sandbodies Extension Index of 50, 80 and 110 and comparable Net-to-Gross ratios.

in Figure 4.4 if the cross-sections of the low Net-to-Gross model are compared with the high Net-to-Gross model. The clay matrix (overbank deposits) act more and more like independent random spots of low permeability within the permeable zones (amalgamated sandstone bodies).

Horizontal Permeability Perpendicular to the Paleo-Flow Direction

The statistical moments of the probability distributions of the horizontal permeability perpendicular and parallel to the paleo-flow direction as a function of sample volume show similar behavior(Figure 4.5 and Figure 4.6), but the flow paths are different. The elongated and continuous shape of a sandstone body, under the assumption that the point bars are connected, supports the permeability parallel to the paleo-flow direction intrinsically (i.e., a flow path is always established in the paleo-flow direction). On the other hand, the width of an isolated sandstone body is restricted by the lateral accretion and amplitude of the river. The mean effective permeability parallel to the paleo-flow direction will therefore converge to the permeability of the overbank deposits if the sample volume increases to the width of the sandstone body. Amalgamation of different sandstone bodies perpendicular to the paleo-flow direction is therefore essential for establishing horizontal flow paths perpendicular to the paleo-flow direction. The amalgamation of sandstone bodies is heavily dependent on the Net-to-Gross ratio. If the Net-to-Gross ratio increases, the chances of amalgamation of one or multiple sandstone bodies increases. Flow paths of amalgamated sandstone bodies are expected to be complex. Flow paths perpendicular to the paleo-flow direction can not only be established with horizontal amalgamation, but also vertically via incision. Generally, flow paths will be established more and more if the Net-to-Gross ratio increases and the flow paths become less tortuous with increasing Net-to-Gross. Figure 4.5b illustrates this behavior with

little decrease of the mean effective permeability perpendicular to the paleo-flow direction with increasing sample volume for high Net-to-Gross ratios and a significant decrease of the mean effective permeability perpendicular to the paleo-flow direction with increasing sample volume for lower Net-to-Gross ratios.

Vertical Permeability

The statistical moments of the probability distributions of the vertical permeability show completely different behavior compared to the horizontal permeability (Figure 4.5c and Figure 4.6c). Still, the behavior is mainly dependent on the Net-to-Gross ratio. This can be explained by the elongated geometry and stacking patterns of sandstone bodies. As mentioned before, low Net-to-Gross ratios result in sandstone bodies that are more or less independent flow paths within the clay matrix (overbank deposits). Even more, if the sandstone bodies are isolated objects and the sample size is large enough, they only support flow parallel to the paleo-flow direction. Therefore, the mean effective vertical permeability will converge to the permeability values of the clay matrix if the sample size increases. Increasing the Net-to-Gross ratio will increase the chance of incision and amalgamation of sandstone bodies. The values for the mean effective vertical permeability at sub-sample size 100 in Figure 4.3 clearly show that the connectivity reduces to the permeability values of the clay matrix for Net-to-Gross ratios below 0.3. If the Net-to-Gross ratio increases, more and more vertical flow pathways are established by amalgamation of the sandstone bodies. Multiple studies (Larue and Hovadik, 2006; Pranter and Sommer, 2011; Willems et al., 2017) have shown that three dimensional connectivity rapidly increases from several percentages to almost 100% connectivity around a Net-to-Gross ratio of 0.3. This is in line with the findings in this study (Figure 4.3). It is shown that the mean effective vertical permeability values at large sample sizes for models with a Net-to-Gross above 0.3 clearly show higher values than the harmonic mean of all the permeability values in the model[1]. Still, the mean effective vertical permeability is low for models with a Net-to-Gross ratio around 0.7 (20mD). A visual inspection of the cross-sections of the model with a Net-to-Gross ratio of 0.69 in Figure 4.4 suggests a higher mean effective vertical permeability. section 4.4 and section 4.5 elaborate on possible explanations for this behavior.

4.3.2 REV, Mean Effective Permeability and Sandstone Bodies Extension Index

The curves of the mean and coefficient of variation of the probability distributions of the effective permeability as a function of sample volume in Figure 4.5 and Figure 4.6 are heavily dependent on the Net-to-Gross ratio, but the geometry of the sandstone bodies can not be neglected. Figure 4.3 visualizes the differences of the mean effective permeability between models with different sandstone body geometries even better. The horizontal permeability parallel to the paleo-flow direction is very similar for all sandstone body geometries. The horizontal permeability perpendicular to the paleo-flow direction shows different behavior. The ribbon type sandstone bodies tend to have a significant lower mean effective horizontal permeability perpendicular to the paleo-flow direction compared to the models with more sheetlike type sandbody geometries. This behavior can be explained with a visual inspection of the cross-sections of two models with a comparable Net-to-Gross ratio, but a different sandstone body geometry (Figure 4.7). The left three cross sections are taken from a model with a ribbon type sandstone body geometry whilst the right three cross-sections are taken from a model with a sheetlike type sandstone body geometry. The horizontal permeability perpendicular to the paleo-flow direction is heavily dependent on lateral amalgamation of sandstone bodies in order to ensure connectivity perpendicular to the paleo-flow direction.

1 The lower bound of the effective permeability of the entire model

If the width of the sandstone bodies is larger, the chances of lateral amalgamation increase. The cross-sections perpendicular to the paleo-flow directions in Figure 4.7 clearly show this. The sandstone bodies of the model with an SEI of 110 are much more amalgamated than the sandstone bodies of the model with an SEI of 50. An important observation from Figure 4.3 is the difference between the curve of the mean effective vertical permeability of the ribbon type deposits (SEI 50) and the curves of the mean effective vertical permeability of the more sheetlike type deposits (SEI 80 and 110). The mean effective vertical permeability of the ribbon type deposits is diverging faster from the harmonic mean of the permeability as a function of Net-to-Gross. This is very likely caused by the sandstone body geometry. If the sandstone bodies are more ribbon type, the volume of a single sandstone body is much smaller than the volume of a sheetlike type sandstone body. This results in more individual sandstone bodies if the models have the same Net-to-Gross ratio. The likelihood of incision and amalgamation therefore increases. This could result in more vertical flow pathways and a higher mean effective vertical permeability.

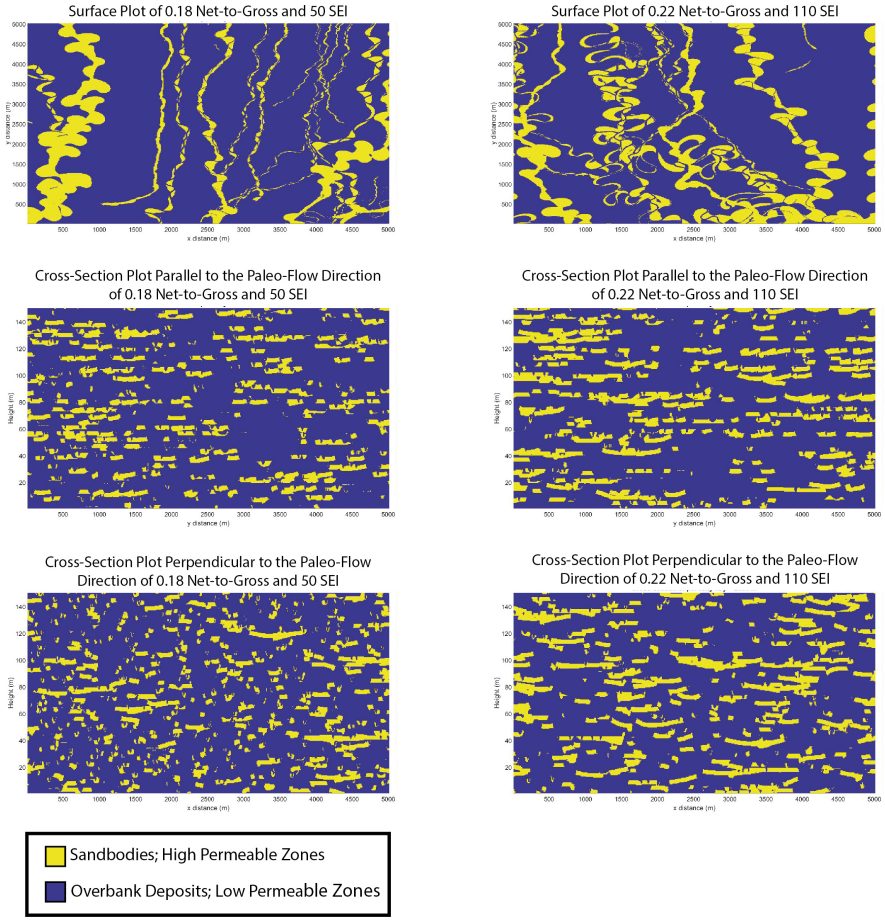

Figure 4.7: A comparison of three cross-sections from two models with a comparable Net-to-Gross ratio, but a large difference in sandstone body geometry. The left cross-sections are taken from a model with a Sandbody Extension Index (SEI) of 50 (ribbon type) and the right cross-sections are taken from a model with a Sandbody Extension Index (SEI) of 110 (sheetlike type). The sheetlike type deposits (right) show more horizontal amalgamation of the sandstone bodies than the ribbon type (left). Especially the cross-sections perpendicular to the paleo-flow direction illustrate the difference of the sandstone body geometry.

4.4 EFFECTIVE PERMEABILITY AND NON-INTUITIVE HETEROGENEITY SCALES

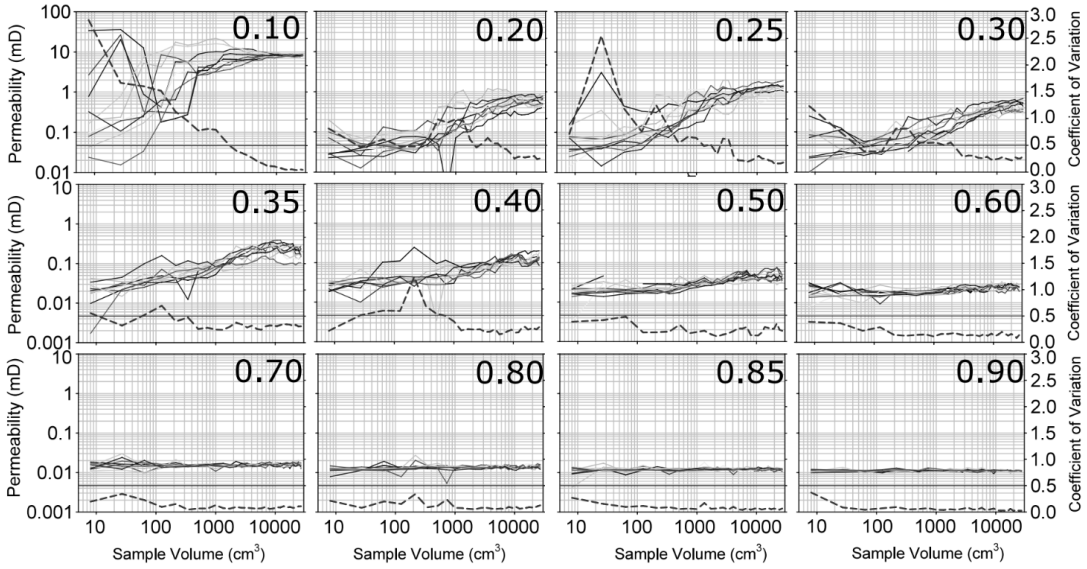

Figure 4.8: This figure shows the vertical permeability from different heterolithic tidal lithofacies models as a function of sample volume from the study of: Nordahl and Ringrose (2008). The number in the upper right corner of each plot shows the mudstone fraction of the lithofacies model. Each model has ten realizations. A sample is taken from the centre of each realization with increasing size. Each line represents the vertical permeability of a single realization with increasing block size. The dashed line is the coefficient of variation of the ten realizations as a function of sample size. All curves show a clear increase in vertical permeability as a function of sample volume for models with a mudstone content below 0.60. Especially the behavior of the models with a mudstone content of 0.10 is particular. A couple of the curves start with a high vertical permeability. The vertical permeability diminishes if the sample volume increases. A further increase in sample size drastically increases the permeability. This behavior is very likely caused by the effects explained in Figure 4.9. Figure from: Nordahl and Ringrose (2008).

Many authors have done analysis on the statistical properties of high permeability contrast deposits (Desbarats, 1987; Deutsch, 1989; Desbarats, 1989; Nordahl et al., 2005; Nordahl and Ringrose, 2008). They all conclude that the vertical permeability is generally underestimated and the horizontal permeability is generally overestimated if the effective permeability is measured below REV. Figure 4.8 shows an example of the effect of sample size on the measurement of vertical permeability of heterolithic tidal depositional models (Nordahl and Ringrose, 2008). On the contrary, the results from this study show that the horizontal permeability and especially the vertical permeability is overestimated if the samples are below REV. An important difference is that measurements from Desbarats (1987); Deutsch (1989); Desbarats (1989); Nordahl et al. (2005); Nordahl and Ringrose (2008) are taken over a volume that has equal sides in all directions. Sedimentological structures, at every scale, are usually wider than long due to the nature of deposition. This is the main reason that almost every sedimentological system has a significantly higher effective horizontal permeability than effective vertical permeability (i.e., the vertical flow pathways, if they even exist, are much more tortuous than the

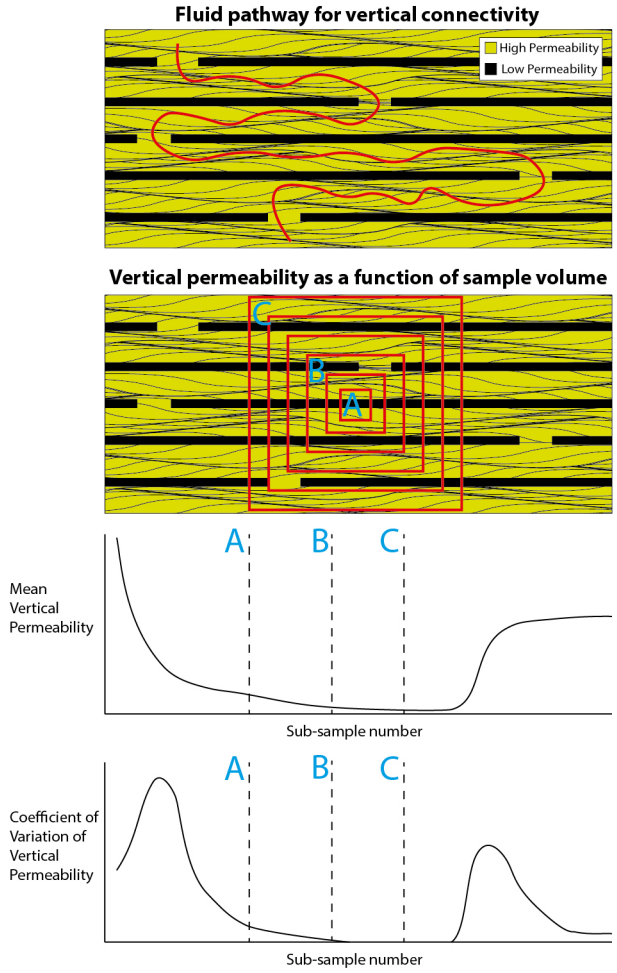

Figure 4.9: The upper picture shows a clear fluid pathway for vertical flow. Although it is tortuous, the vertical permeability will clearly not tend toward the the low permeability values. If we would sample from random locations with a small sample size, the mean of the vertical permeability will be high, because many samples do not catch the clay layers. If the size increases, the likelihood of capturing both the high permeable and low permeable layers in one sample increases and the mean of the sub-samples decreases. Because the drop of the mean is steeper than the decline in standard deviation, the coefficient of variation increases first with sampling size. With the sub-sample size increasing more and more the decline of the mean gets less than the decline of the standard deviation and the coefficient of variation decreases. If the sample size is large enough that it always captures at least two low permeable layers (B), the mean of the sub-samples will be mainly dependent on the low permeable layers (i.e., the low permeable layers seem to act as barriers to vertical flow.). This results in a coefficient of variation that is reduced to zero and a constant mean that tends towards the low permeability values. The system seems to have reached all criteria for REV. Nevertheless, if we increase the sub-sample size such that it is larger than the size of sub-sample size C, at a certain point the mean of the vertical permeability will increase as does the coefficient of variation. This is caused by the fact that the sub-sample size is now able to capture a full flow path and the low permeable layers rather act as baffles than barriers.

horizontal flow pathways). Due to the regular ways of measuring permeability in core plugs (sealed side permeability measurement) and upscaling (sealed sides boundary conditions or periodic boundary conditions), vertical permeability is generally underestimated (very tortuous flow pathways are not captured and baffles act as barriers) and horizontal permeability is generally overestimated (barriers and baffles to horizontal flow are not captured resulting in less tortuous flow pathways than in reality). An example of the effect of thickening barriers and missing tortuous flow pathways on the vertical permeability is shown and explained in Figure 4.9. It is easy to imagine that the mean effective permeability will always be maximal if the sample size is infinitely small. This has been shown in Figure 4.1. An increase in sample size will generally result in a decrease of the mean effective permeability perpendicular to the layering of the model (Figure 4.9). At a certain sample size, the mean of the effective permeability could potentially become constant as the sample size increases. Still, the 'true' effective permeability could not yet been reached. The baffles act as barriers at this sub-sample size and if the sample volume is increased or elongated in the horizontal direction, the mean of the vertical permeability will suddenly increase. This shows that the REV (or length scale of the heterogeneity) can be not intuitively clear from the the statistical moments (or model). This hypothesis can be tested using the data of the vertical permeability of (Nordahl and Ringrose, 2008) shown in Figure 4.8. All curves clearly show an increase in vertical permeability as a function of sample volume. The behavior of the curves of the realizations with a mudstone content of 0.10 are very distinctive. Some of the realizations have high permeability with small sample sizes. An increase in sample size results in a decrease in vertical permeability. If the sample size is further increased the vertical permeability goes up again until it reaches a constant value. This behavior is perfectly in line with the behavior of the mind experiment in Figure 4.9. The models with higher mudstone contents have more baffles. This could cause even the smaller measurements to always capture a mudstone layer. Increasing the sample size results in capturing more and more of the tortuous flow pathways.

4.4.1 Fluvial Depositional Models and Vertical Permeability

The explanation for the difference between the results of this study and the studies of Desbarats (1987); Deutsch (1989); Desbarats (1989); Nordahl et al. (2005); Nordahl and Ringrose (2008) is twofold. At first, the geometry of the sandstone bodies and the stacking pattern of fluvial systems is different from the behavior of small scale sedimentary structures. This results in different permeable zone geometries and could potentially have a different effect on the behavior of the vertical permeability as a function of sample size. The second reason for the differences could be caused by the shape of the samples. This study uses cells and subsamples that are 20 times as wide as thick. The likelihood of sampling the whole vertical flow pathway becomes therefore larger and the samples are less likely to capture barriers as baffles. This could cause the mean to show only monotonic decline of the vertical permeability with an increase in sample size. Still, analysis of the high Net-to-Gross models (Net-to-Gross around 0.7) shows that the mean effective vertical permeability at large sub-samples (> 80) is around 20mD. This number seems low if we visually inspect the cross-sections from the model in Figure 4.4 and Figure 4.10. A possible explanation for a lower mean effective permeability than expected could be due to baffles that act as barriers at the scale of the largest sub-sample size (i.e., 1000m x 1000m x 50 m). Figure 4.10 shows an example of potential flow barriers/baffles in a high Net-to-Gross model. The example in Figure 4.9 is identical to how these elongated patches of clay matrix can affect the behavior statistical moments of the probability distributions of the vertical permeability. This shows that the vertical permeability decreases for sub-samples up to 1000m x 1000m x 50m, but the vertical permeability could certainly increase if sub-samples are larger. Sampling at larger sub-sample sizes could confirm or reject this hypothesis.

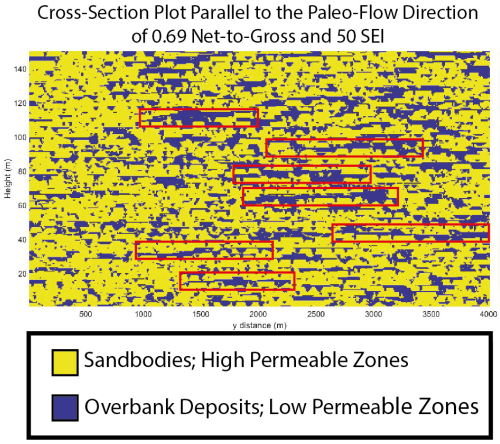

Figure 4.10: The figure shows a cross section of a model parallel to the paleo-flow direction with a Net-to-Gross ratio of 0.69. The red boxes show examples of continuous patches of clay matrix that are longer than the largest sub-sample size (1000m). The barriers/baffles are generally less extensive perpendicular to the flow direction so that they would act as baffles rather than barriers. The figure illustrates the mind experiment explained in Figure 4.9 and its potential influence on the mean effective vertical permeability. The mean effective vertical permeability determined in Figure 4.3 could well be higher if the sample size is further increased.

4.5 REV AND THE SHAPE OF SUB-SAMPLE VOLUMES

The difference between the results of Desbarats (1987); Deutsch (1989); Desbarats (1989); Nordahl et al. (2005); Nordahl and Ringrose (2008) and this study shows that the expected value of the effective vertical permeability as a function of sub-sample volume can be dependent on both the geometry of the permeability field of the sample space and the shape of the sub-sample volume. Figure 4.9 clearly visualizes why the shape of the sub-sample size has a large influence on the effective permeability as a function of sub-sample volume with respect to the heterogeneity scales. If the shape sub-sample volume would have been much more elongated, both the expected value of the effective permeability and the coefficient of variation as a function of sub-sample size would have been significantly different. The shape of the sub-sample volume could potentially be made elongated enough that the curve of the expected vertical permeability would only decrease as a function of sub-sample size and the coefficient of variation would not reach zero without capturing the REV of the large heterogeneity scale. This theory is mainly valid for a layered system, especially if there are no major baffles for horizontal flow that can act as barriers if the the sub-sample size is too small. Figure 4.11 shows the effective permeability as a function of sub-sample size in the strict definition of REV. This figure shows clearly that a heterogeneity scale is missed if the sub-sample size is a square or a cube. An elongated sub-sample volume would be more likely to capture the small scale heterogeneity REV. The considerations above suggest that it is better to use elongated sub-sample volumes for REV estimation in layered systems, because they are generally better able to capture the heterogeneity of geometry than sub-samples with equal sides. It is very difficult to obtain the length scales of the heterogeneity's intuitively, but these examples and the results from this study show that this sub-sampling method pays more respect to the intrinsic geometry of the layered systems.

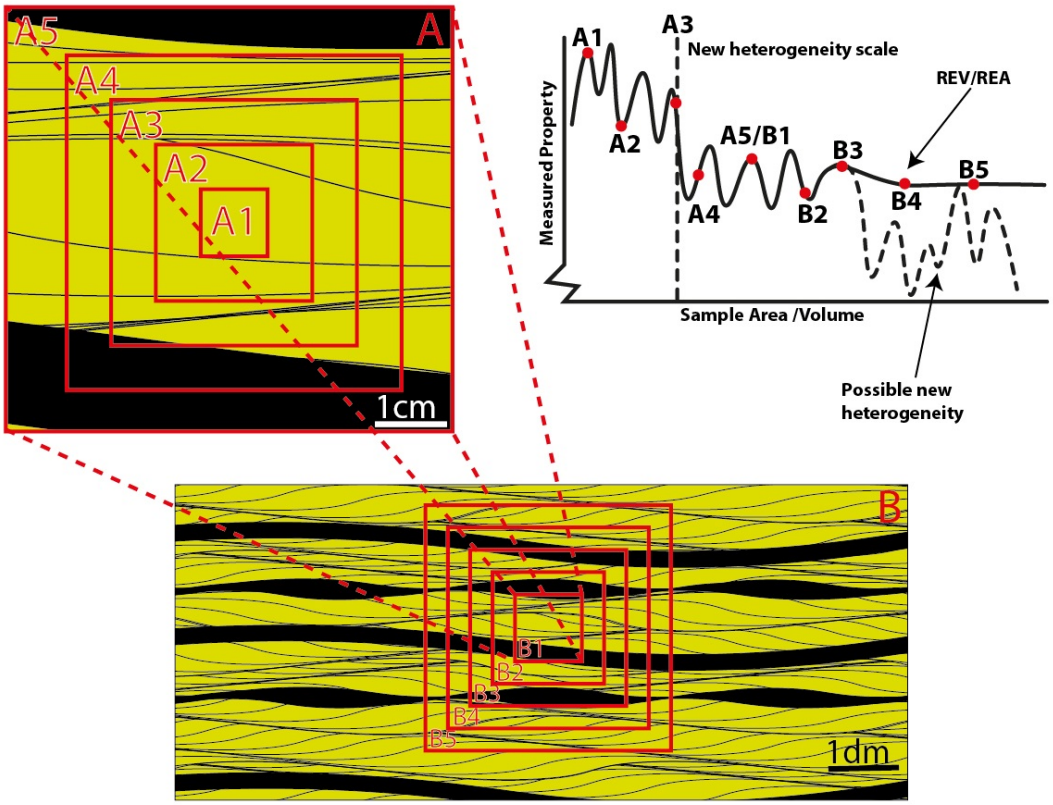

Figure 4.11: Figure A shows a small scale heterogeneity if we assume that the bedding structures (small black lines) represent minor baffles to flow. Figure B shows the large scale heterogeneity scale with the high permeable cross-bedded sands and low permeable clay intercalations. If the small scale heterogeneity is sampled for effective vertical permeability, the effective vertical permeability varies if more and more of the complex bedding structures are captured. As the sub-sample volume is increased, at a certain point the new heterogeneity scale is captured and the vertical permeability is drastically decreased. It still varies and will either reach REV if the sub-sample size is further increased or reaches a possible new heterogeneity scale. The graph shows that expected property as a function of sample volume.

4.6 UPSCALING AND SAMPLE SIZE STATISTICS

The influence of the geometry of the high permeable zones (sandstone bodies) on the REV and effective properties of a porous medium is clear from Figure 4.1, Figure 4.9 and Figure 4.11. The complexity of flow paths through porous media at all heterogeneity scales forms the main basis of the research on REV. The main goal of research on permeable media, from the first experiments with permeability of Henry Darcy in 1856 to very complex multi-phase flow models of today, is to produce a realistic response output for flow of fluids through a porous medium. Lack of computational power and the inability to describe the flow of fluids in porous media into detail physically is and always has been the reason to simplify fluid flow through porous media with effective parameters such as permeability and porosity. If it would be possible to describe the response output of the reservoir at the size of the pore level, induced by any configuration of injection and/or production wells

in a reservoir, this would always be preferable; this is certainly not the case. Even more, a coarse scale dynamic reservoir model generally has grid cells between 50 and 200 meters in length and are generally 0.5 to 5 metres thick. The coarse scale dynamic model is derived from upscaling of a fine scale static model. This study shows that the expected value of both vertical and horizontal permeability would be overestimated if the the size and shape of the grid cells is the same as used in this study and the cells are upscaled with single-phase flow-based permeability upscaling with sealed sides boundary conditions. The overestimation will generally be less with higher Net-to-Gross ratios. It must be noted that the spatial distribution of the coarse grid cells with the effective properties will restrict the overestimation of the permeability of the entire reservoir (i.e., the new coarse scale heterogeneous permeability field induces new restrictions to flow that generally decrease the effective permeability of the entire reservoir). Other upscaling methods for both single and multi-phase flow exist (Wen and Gómez-Hernández, 1996; Durlofsky, 2005). Many of the upscaling methods, such as regional and global upscaling capture the surrounding geometry around the upscaled cell. The surrounding geometry is used to obtain a better estimate of the response of the flow cell including the effect of the surrounding cells or the entire sample space on the boundary conditions imposed on the flow cell (Durlofsky, 2005). Still, problems exist with upscaling, because the size of the upscaled cell is not inevitably clear from the model. The statistical moments of the probability distributions of permeability as a function of sample size and especially the sample size where the expected value of the effective permeability does not vary with increasing sample size could potentially serve as a test for the relevant spatial scale of upscaling.

4.7 APPLICATIONS OF REV AND EFFECTIVE PROPERTY ESTIMATION

This study shows that fluvial depositional systems can be analyzed with REV theory and the determination of effective properties can be used to estimate the effective properties. Still, the applications of the methods are different compared to REV theory and determination of effective properties at the pore or bedding scale. section 4.6 briefly elaborates on the potential of REV theory for determining a relevant spatial scale for upscaling. But the potential of this theory could have other applications. Sanei and Fertig (2015) have done research on variability of the fiber volume fraction in fiber reinforced polymers. This study shows that the REV of fiber reinforced polymers is generally larger than the assumed to be homogeneous cell size. One of his most important findings dealt with the spatial relationships of cells with varying sizes. The study shows that it is possible to find a cell size where there is still variability between the different sub-samples (i.e., REV is not reached), but the measured cell properties become uncorrelated with respect to their neighboring cells (Sanei and Fertig, 2015). If there would exist such a scale for fluvial depositional models that is smaller than the REV, this could drastically simplify the population of properties of fluvial reservoir models. This could mean that that the knowledge of the variability and the mean of the permeability at a certain scale are the only two parameters needed to obtain a reasonably accurate and statistically accurate reservoir model. It could potentially be used if we would like to obtain models for reservoirs where we do not have extensive knowledge or where there is no time and money for extensive reservoir modeling. The input models for the analysis of the statistical moments of the permeability, as well as other non-additive properties that would be needed to simulate a reservoir (water saturation, relative permeability, etc.), need to be accurate in order to obtain realistic results. Heterogeneity and statistics at the wells could potentially be included specifically in order to address the uncertainty at the well.

5 CONCLUSIONS

Fluvial reservoirs are difficult to model due to the high permeability contrasts between the sandstone bodies and the overbank deposits and the complex geometry of the permeable (sandstone bodies) and impermeable zones (overbank deposits). The concept of REV has proven to be a successful method for the determination of effective properties such as porosity and permeability in heterogeneous high permeability/porosity contrast sedimentary deposits. The statistical moments of the probability distributions of porosity and permeability as a function of sample volume have been determined for synthetic models of fluvial depositional systems. The curves of the statistical moments have been analyzed for different Net-to-Gross ratios and different sandstone body geometries. This study helps to get a better understanding of the effect of the geometry of permeable zones in a fluvial depositional system on the size of an upscaled cell.

The main results from this study are:

- It is shown that a fluvial depositional system can be analyzed by the statistical moments of the probability distributions of porosity and permeability as a function of sample volume. A sample space at the scale of a depositional system does not react significantly different than analysis that has been done on smaller scales (Bachmat and Bear, 1986, 1987; Deutsch, 1989; Desbarats, 1989; Nordahl and Ringrose, 2008; Nordahl et al., 2014). The main difference between the studies of small scale heterogeneities and this study is the behavior of the mean vertical permeability as a function of sample volume. This study shows that the vertical permeability is overestimated with small sample sizes, while all studies of small scale heterogeneities show that the mean vertical permeability is overestimated with small sample sizes. The reason for this difference could be twofold. At first, it could be an effect of the differences between the geometries of small scale sedimentary structures and geometries of sandstone bodies in fluvial depositional systems. At second, it could be an effect of the shape of sub-samples. The sub-samples in this study are more elongated in the horizontal direction, compared to square and cubic samples in studies of smaller sedimentary structures.
- It is shown that the statistical moments of the effective properties as a function of sample size relate to properties like Net-to-Gross and the geometry of sandstone bodies. Net-to-Gross is the most important parameter for the effective properties. The sandstone body geometry is an important parameter for the horizontal permeability perpendicular to paleo-flow direction. Sandstone bodies with a more sheetlike type geometry show significant higher horizontal permeability perpendicular to paleo-flow than sandstone bodies with a ribbon type geometry. On the contrary, sandstone bodies with a more ribbon type geometry show a slightly higher vertical permeability compared to models with a more sheelike type geometry.
- All models show that the expected value of the permeability as a function of sub-sample size tends to be independent from the sub-sample size if it is larger than a certain value. Even more, the convergence of the expected value of the permeability as a function of

sample value occurs much earlier than the convergence of the variability. This indicates that it might be possible to say something about the true effective properties based on the statistical moments of probability distributions as a function of sub-sample size at REV, without reaching REV.

- The REV analysis of fluvial depositional shows potential applications for modeling of fluvial reservoirs. The determination of the relevant spatial scale of upscaling from the static (fine scale) to the dynamic (coarse scale) model is difficult (de Hoop, 2017). Analysis of the convergence of the mean effective permeability as a function of sample volume could potentially serve as a test for the determination of the relevant spatial scale. A second potential application is the simplification of modeling of fluvial reservoirs. If the mean of the effective permeability does not change with sample volume and the cells are uncorrelated with respect to neighboring cells, fluvial reservoirs can potentially be modeled with the statistical moments of the effective properties (Sanei and Fertig, 2015). Further research is needed to evaluate the potential.

BIBLIOGRAPHY

Bachmat, Y. and Bear, J. (1986). Macroscopic modelling of transport phenomena in porous media. 1: The continuum approach. *Transport in porous media*, 1(3):213–240.

Bachmat, Y. and Bear, J. (1987). On the concept and size of a representative elementary volume (REV). In *Advances in transport phenomena in porous media*, pages 3–20. Springer.

Bear, J. (1972). Dynamics of fluids in porous materials. *Society of Petroleum Engineers*.

Begg, S. and King, P. (1985). Modelling the Effects of Shales on Reservoir Performance: Calculation of Effective Vertical Permeability. In *SPE Reservoir Simulation Symposium*. Society of Petroleum Engineers.

Carman, P. C. (1937). Fluid flow through granular beds. *Trans. Inst. Chem. Eng.*, 15:150–166.

Chen, C., Hu, D., Westacott, D., and Loveless, D. (2013). Nanometer-scale characterization of microscopic pores in shale kerogen by image analysis and pore-scale modeling. *Geochemistry, Geophysics, Geosystems*, 14(10):4066–4075.

Corbett, P. and Jensen, J. (1992). Estimating the mean permeability: how many measurements do you need? *First Break*, 10(1253):89–94.

Dagan, G. (1979). Models of groundwater flow in statistically homogeneous porous formations. *Water Resources Research*, 15(1):47–63.

Darcy, H. P. G. (1856). *Les Fontaines publiques de la ville de Dijon. Exposition et application des principes à suivre et des formules à employer dans les questions de distribution d'eau, etc*. V. Dalamont.

de Hoop, S. (2017). *Determination of Relevant Spatial Scale in Reservoir Simulation*. PhD thesis, Delft University of Technology.

Desbarats, A. (1989). Support effects and the spatial averaging of transport properties. *Mathematical Geology*, 21(3):383–389.

Desbarats, A. J. (1987). Numerical estimation of effective permeability in sand-shale formations. *Water Resources Research*, 23(2):273–286.

Deutsch, C. (1989). Calculating Effective Absolute Permeability in Sandstone/Shale Sequences. *SPE Formation Evaluation*, 4(03):343–348.

Donselaar, M. E. and Overeem, I. (2008). Connectivity of fluvial point-bar deposits: An example from the Miocene Huesca fluvial fan, Ebro Basin, Spain. *AAPG Bulletin*, 92(9):1109–1129.

Durlofsky, L. J. (1991). Numerical calculation of equivalent grid block permeability tensors for heterogeneous porous media. *Water Resources Research*, 27(5):699–708.

Durlofsky, L. J. (2005). Upscaling and gridding of fine scale geological models for flow simulation. In *8th International Forum on Reservoir Simulation Iles Borromees, Stresa, Italy*, volume 2024, pages 1–59.

FLUMY® (2017). ARMINES FLUMY®\ Project Users Guide.

Haldorsen, H. H. (1986). Simulator parameter assignment and the problem of scale in reservoir engineering. *Reservoir characterization*, 6.

Hartkamp-Bakker, C. A. and Donselaar, M. E. (1993). Permeability patterns in point bar deposits: Tertiary Loranca Basin, central Spain. *The Geological Modelling of Hydrocarbon Reservoirs and Outcrop Analogues*, pages 157–168.

Holden, L. and Nielsen, B. F. (2000). Global Upscaling of Permeability in Heterogeneous Reservoirs; The Output Least Squares (OLS) Method. *Transport in Porous Media*, 40(2):115–143.

Howell, J. A., Martinius, A. W., and Good, T. R. (2014). The application of outcrop analogues in geological modelling: A review, present status and future outlook. *Geological Society, London, Special Publications*, 387(1):1–25.

Hubbert, M. K. (1956). Darcy's Law and the Field Equations of the Flow of Underground Fluids. *A.I.M.E. Petroleum Transactions*.

Hurst, A. (2009). Sedimentary Flow Units in Hydrocarbon Reservoirs: Some Shortcomings and a Case for High-Resolution Permeability Data. In *The Geological Modelling of Hydrocarbon Reservoirs and Outcrop Analogues*, pages 189–204. Blackwell Publishing Ltd., Oxford, UK.

Indelman, P. and Dagan, G. (1993). Upscaling of Permeability of Anisotropic Heterogeneous Formations 1. The General Framework. Technical Report 4, Tel Aviv University, Tel Aviv.

Jungreuthmayer, C., Steppert, P., Sekot, G., Zankel, A., Reingruber, H., Zanghellini, J., and Jungbauer, A. (2015). The 3D pore structure and fluid dynamics simulation of macroporous monoliths: High permeability due to alternating channel width. *Journal of Chromatography A*, 1425:141–149.

Keogh, K. J., Leary, S., Martinius, A. W., Scott, A. S. J., Riordan, S., Viste, I., Gowland, S., Taylor, A. M., and Howell, J. (2014). Data capture for multiscale modelling of the Lourinhã Formation, Lusitanian Basin, Portugal: an outcrop analogue for the Statfjord Group, Norwegian North Sea. *Geological Society, London, Special Publications*, 387(1):27–56.

Keogh, K. J., Martinius, A. W., and Osland, R. (2007). The development of fluvial stochastic modelling in the Norwegian oil industry: A historical review, subsurface implementation and future directions. *Sedimentary Geology*, 202(1):249–268.

King, M. and Mansfield, M. (1999). Flow Simulation of Geologic Models. *SPE Reservoir Evaluation & Engineering*, 2(04):351–367.

Kozeny, J. (1927). Uber kapillare leitung der wasser in boden. *Royal Academy of Science, Vienna, Proc. Class I*, 136:271–306.

Labourdette, R. (2008). LOSCS Lateral Offset Stacked Channel Simulations: Towards geometrical modelling of turbidite elementary channels. *Basin Research*, 20(3):431–444.

Larue, D. K. and Hovadik, J. (2006). Connectivity of channelized reservoirs: a modelling approach. Technical report, Geological Society of London.

Li, D., Cullick, A., and Lake, L. (1995). Global scale-up of reservoir model permeability with local grid refinement. *Journal of Petroleum Science and Engineering*, 14(1-2):1–13.

Matheron, G. (1967). Kriging or polynomial interpolation procedures. *CIMM Transactions*, 70:240–244.

Matthews, J. D., Carter, J. N., Stephen, K. D., Zimmerman, R. W., Skorstad, A., Manzocchi, T., and Howell, J. A. (2008). Assessing the effect of geological uncertainty on recovery estimates in shallow-marine reservoirs: the application of reservoir engineering to the SAIGUP project. *Petroleum Geoscience*, 14(1):35–44.

Nordahl, K., Messina, C., Berland, H., Rustad, A. B., and Rimstad, E. (2014). Impact of multiscale modelling on predicted porosity and permeability distributions in the fluvial deposits of the Upper Lunde Member (Snorre Field, Norwegian Continental Shelf). *Geological Society, London, Special Publications*, 387(1):85–109.

Nordahl, K. and Ringrose, P. S. (2008). Identifying the Representative Elementary Volume for Permeability in Heterolithic Deposits Using Numerical Rock Models. *Math Geosci*, 40:753–771.

Nordahl, K., Ringrose, P. S., and Wen, R. (2005). Petrophysical characterization of a heterolithic tidal reservoir interval using a process-based modelling tool. *Petroleum Geoscience*, 11(1):17–28.

Norris, R. and Lewis, J. (1991). The Geological Modeling of Effective Permeability in Complex Heterolithic Facies. In *SPE Annual Technical Conference and Exhibition*. Society of Petroleum Engineers.

PetroWiki (2015). Upscaling of Grid Properties in Reservoir Simulation.

Pettijohn, F. J., Potter, P. E., and Siever, R. (1973). Sand and Sandstone. *Springer-Verlag, New York, Heidelberg, Berlin*.

Pranter, M. J. and Sommer, N. K. (2011). Static connectivity of fluvial sandstones in a lower coastal-plain setting: An example from the Upper Cretaceous lower Williams Fork Formation, Piceance Basin, Colorado. *AAPG Bulletin*.

Ringrose, P., Pickup, G., Jensen, J., and Forrester, M. (1999). The Ardross Reservoir Gridblock Analog: Sedimentology, Statistical Representivity, and Flow Upscaling. In R. Schatzinger and J. Jordan, editor, *Reservoir Characterization-Recent Advances*, chapter 18, pages 265–275. AAPG Special Volumes, Edinburgh, Scotland, U.K., aapg memoir 71, edition.

Ringrose, P. S., Martinius, A. W., and Alvestad, J. (2008). Multiscale geological reservoir modelling in practice. *Geological Society, London, Special Publications*, 309(1):123–134.

Ruivo, F. M., Morooka, C. K., and others (2001). Decommissioning Offshore Oil and Gas Fields. In *SPE Annual Technical Conference and Exhibition*.

Sahimi, M. and Islam, M. R. (1996). Flow and Transport in Porous Media and Fractured Rocks. *Journal of Petroleum Science and Engineering*, 16(1):181.

Sanei, S. H. R. and Fertig, R. S. (2015). Uncorrelated volume element for stochastic modeling of microstructures based on local fiber volume fraction variation. *Composites Science and Technology*, 117:191–198.

Tsuji, T., Jiang, F., and Christensen, K. T. (2016). Characterization of immiscible fluid displacement processes with various capillary numbers and viscosity ratios in 3D natural sandstone. *Advances in Water Resources*, 95:3–15.

Warren, J. and Price, H. (1961). Flow in Heterogeneous Porous Media. *Society of Petroleum Engineers Journal*, 1(03):153–169.

Weber, K. (1982). Influence of Common Sedimentary Structures on Fluid Flow in Reservoir Models. *Journal of Petroleum Technology*, 34(03):665–672.

Weber, K. J. (1986). How heterogeneity affects oil recovery. *Reservoir Characterisation: Orlando, Florida*, pages 487–544.

Wen, X. H., Durlofsky, L. J., and Edwards, M. G. (2003). Upscaling of Channel Systems in Two Dimensions Using Flow-Based Grids. *Transport in Porous Media*, 51(3):343–366.

Wen, X.-H. and Gómez-Hernández, J. (1996). Upscaling hydraulic conductivities in heterogeneous media: An overview. *Journal of Hydrology*, 183(1-2):ix–xxxii.

Willems, C. J., Nick, H. M., Donselaar, M. E., Weltje, G. J., and Bruhn, D. F. (2017). On the connectivity anisotropy in fluvial Hot Sedimentary Aquifers and its influence on geothermal doublet performance. *Geothermics*, 65:222–233.

A MEAN, STANDARD DEVIATION AND COEFFICIENT OF VARIATION OF POROSITY AS A FUNCTION OF SAMPLE SIZE

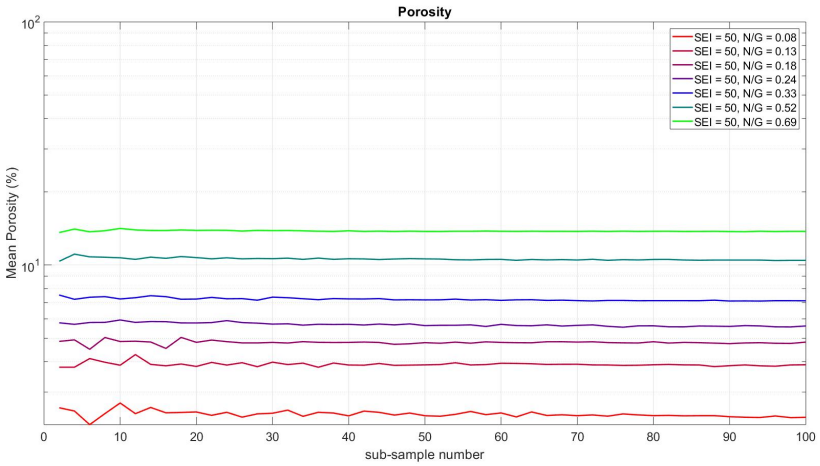

(a) The mean of the porosity as a function of sample volume for models with a Sandbodies Extension Index of: 50.

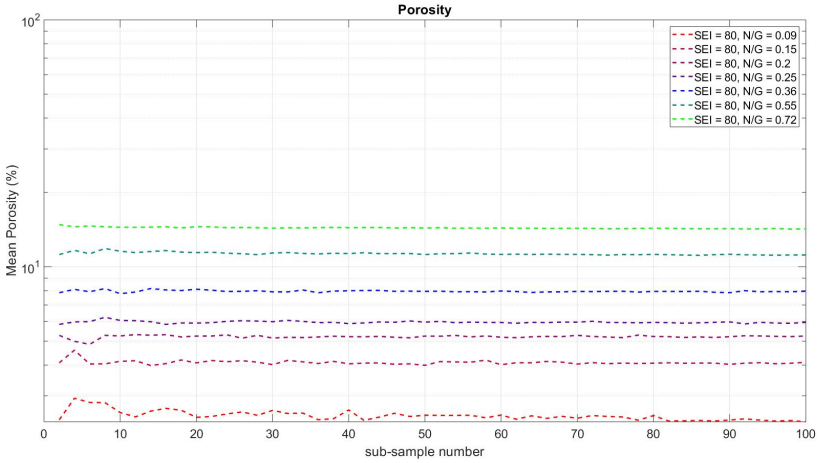

(b) The mean of the porosity as a function of sample volume for models with a Sandbodies Extension Index of: 80.

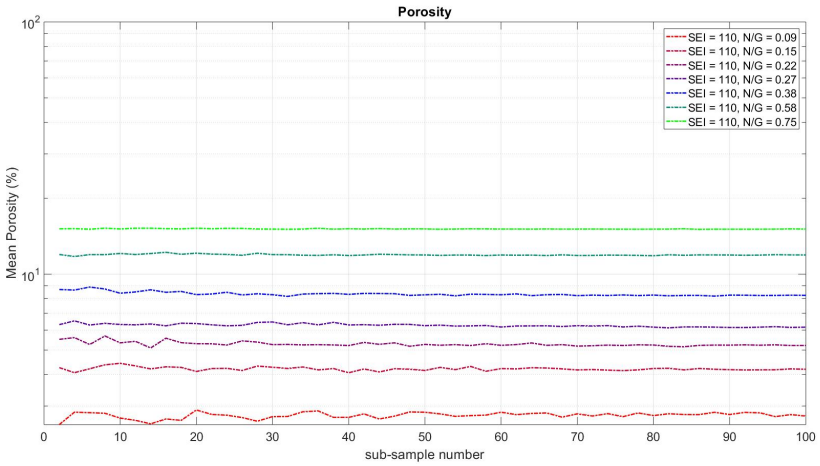

(c) The mean of the porosity as a function of sample volume for models with a Sandbodies Extension Index of: 110.

Figure A.1: The mean of the porosity as a function of sample volume.

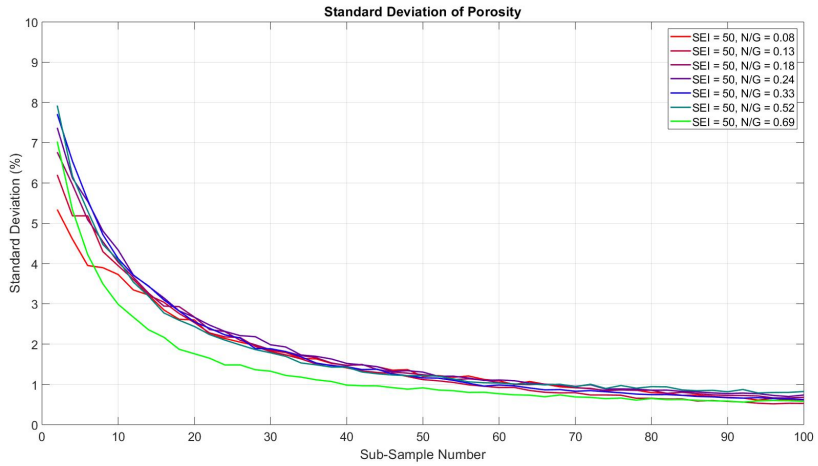

(a) The standard deviation of the porosity as a function of sample volume for models with a Sandbodies Extension Index of: 50.

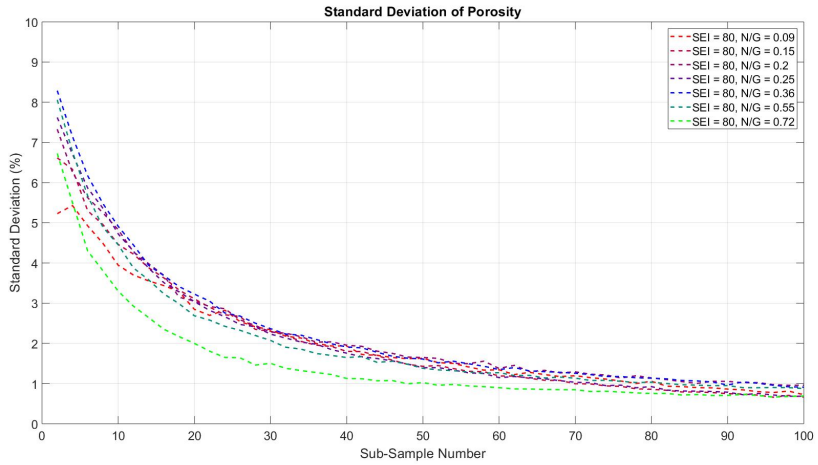

(b) The standard deviation of the porosity as a function of sample volume for models with a Sandbodies Extension Index of: 80.

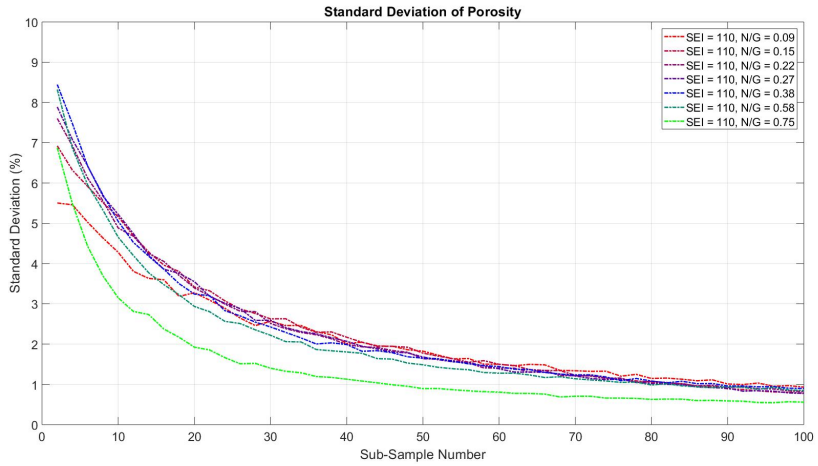

(c) The standard deviation of the porosity as a function of sample volume for models with a Sandbodies Extension Index of: 110.

Figure A.2: The standard deviation of the porosity as a function of sample volume.

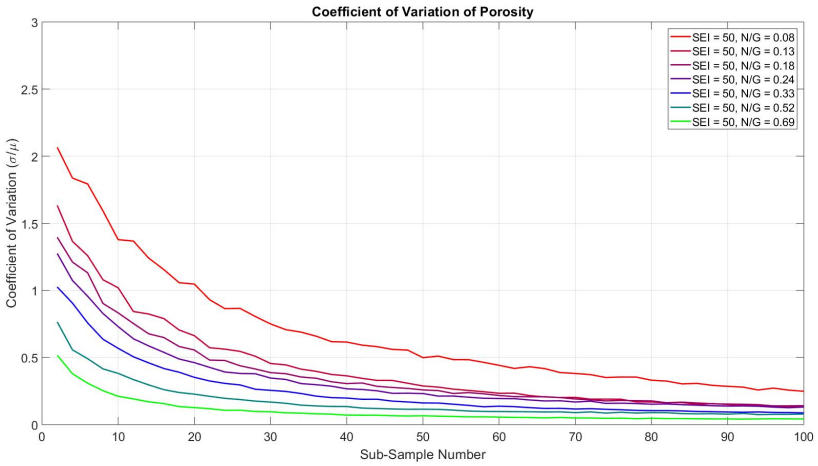

(a) The coefficient of variation of the porosity as a function of sample volume for models with a Sandbodies Extension Index of: 50.

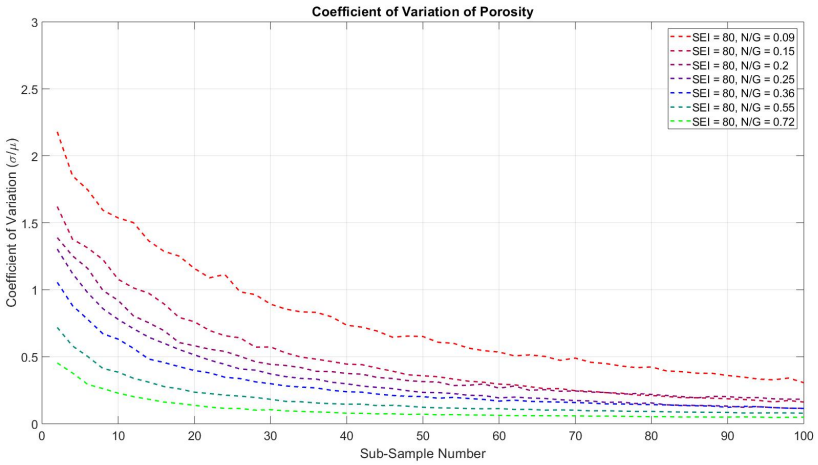

(b) The coefficient of variation of the porosity as a function of sample volume for models with a Sandbodies Extension Index of: 80.

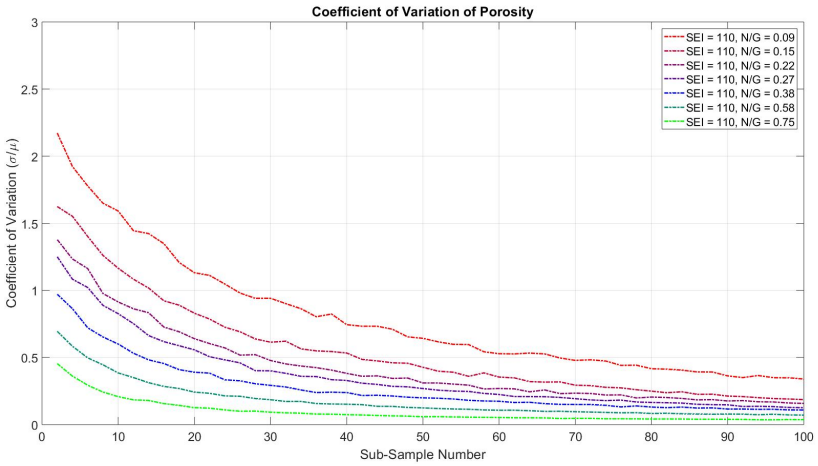

(c) The coefficient of variation of the porosity as a function of sample volume for models with a Sandbodies Extension Index of: 110.

Figure A.3: The coefficient of variation of the porosity as a function of sample volume.

B MEAN, STANDARD DEVIATION AND COEFFICIENT OF VARIATION OF PERMEABILITY AS A FUNCTION OF SAMPLE SIZE

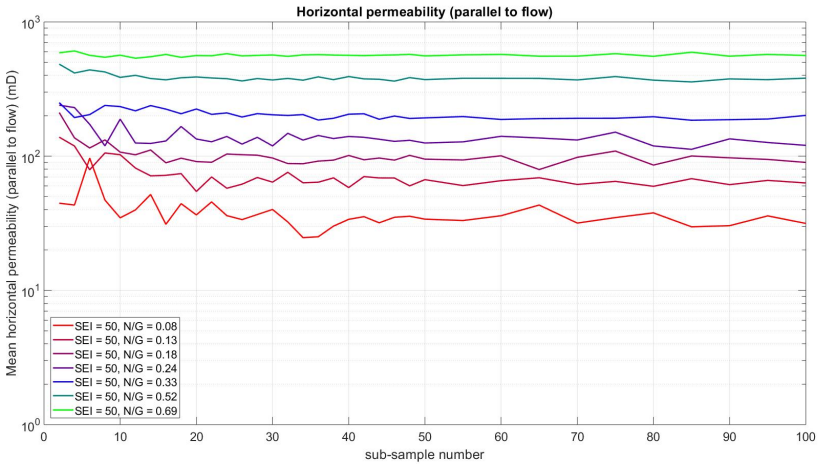

(a) The mean of the horizontal permeability parallel to the paleo-flow direction.

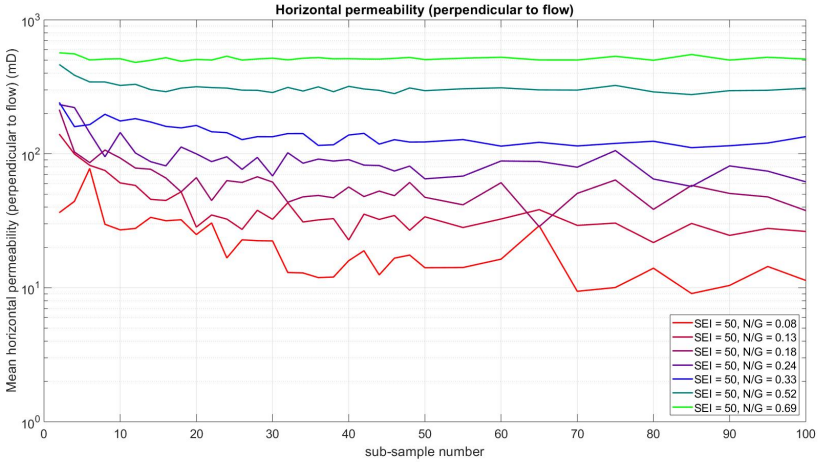

(b) The mean of the horizontal permeability perpendicular to the paleo-flow direction.

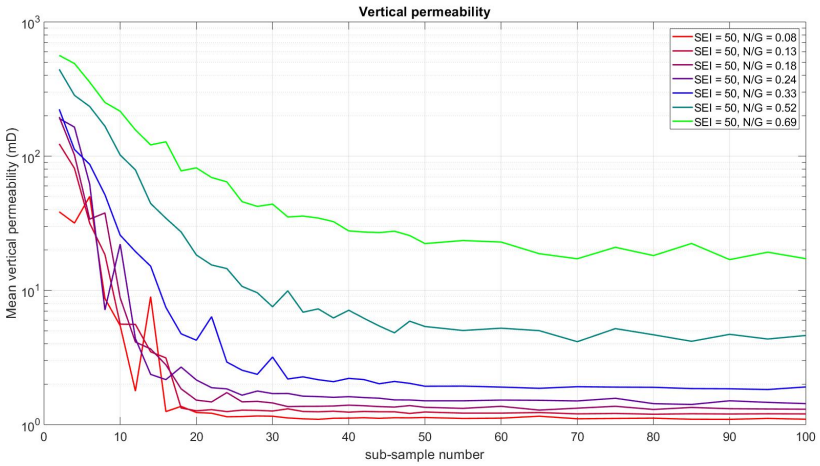

(c) The mean of the vertical permeability.

Figure B.1: The mean of the permeability as a function of sample volume for models with a Sandbodies Extension Index of: 50.

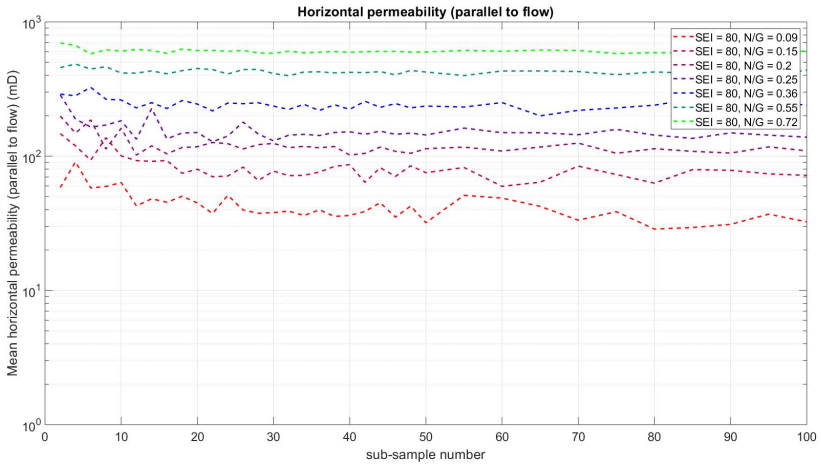

(a) The mean of the horizontal permeability parallel to the paleo-flow direction.

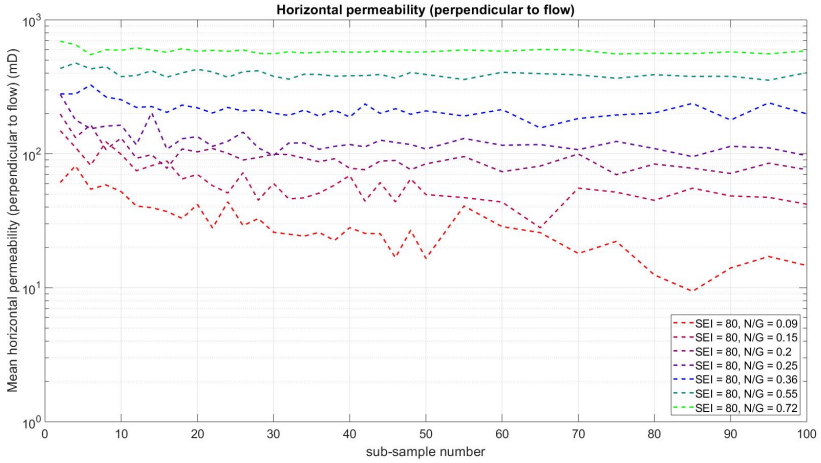

(b) The mean of the horizontal permeability perpendicular to the paleo-flow direction.

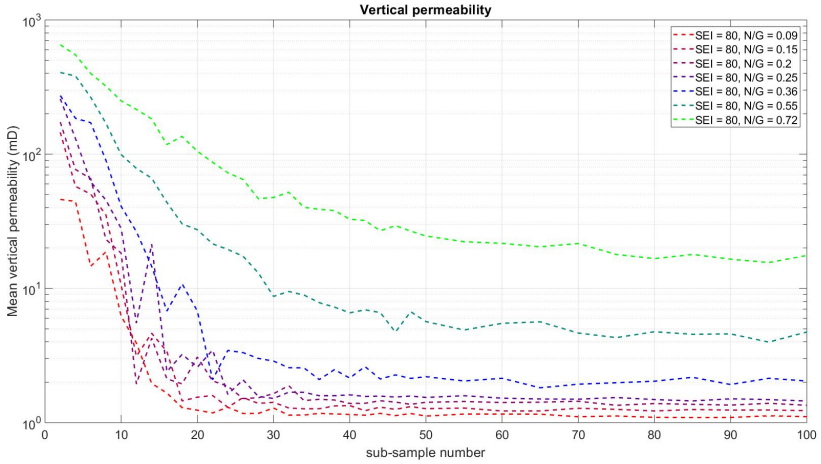

(c) The mean of the vertical permeability.

Figure B.2: The mean of the permeability as a function of sample volume for models with a Sandbodies Extension Index of: 80.

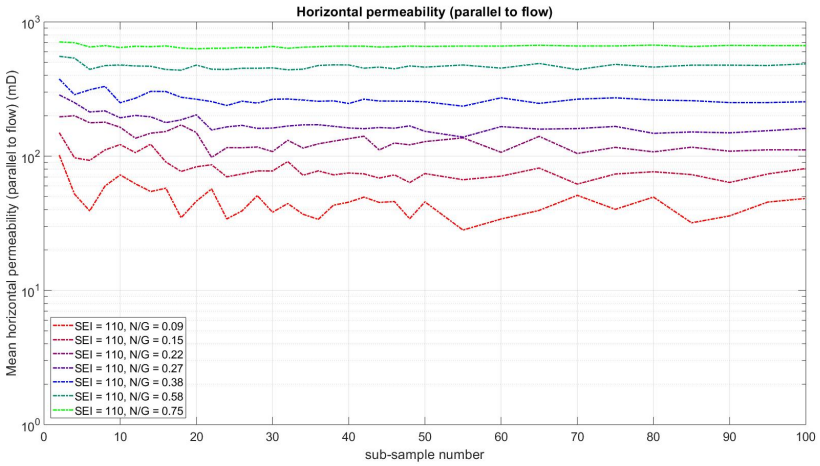

(a) The mean of the horizontal permeability parallel to the paleo-flow direction.

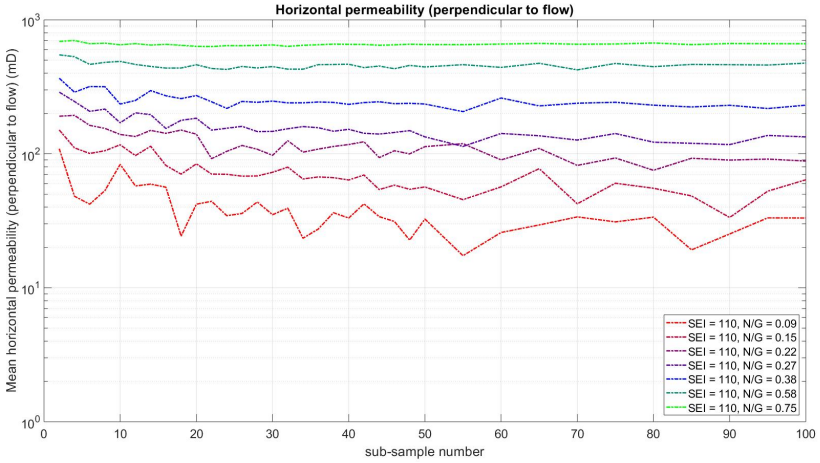

(b) The mean of the horizontal permeability perpendicular to the paleo-flow direction.

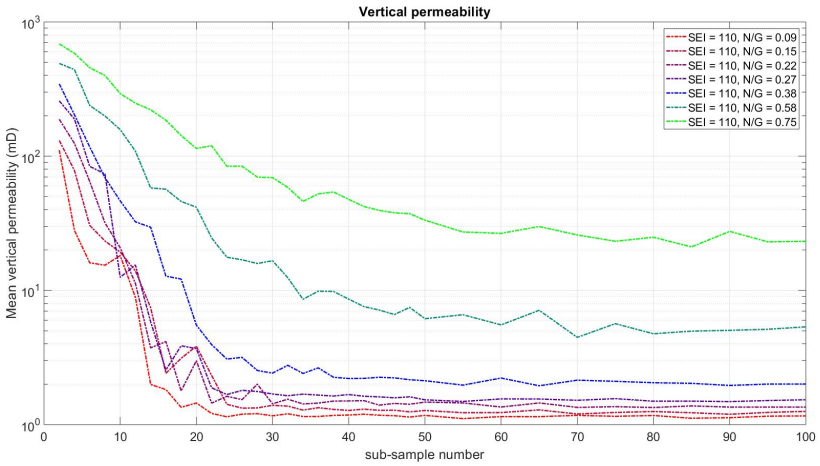

(c) The mean of the vertical permeability.

Figure B.3: The mean of the permeability as a function of sample volume for models with a Sandbodies Extension Index of: 110.

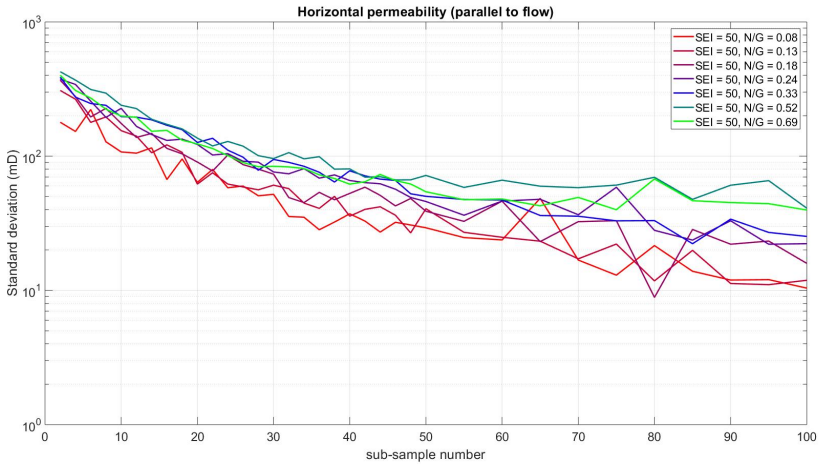

(a) The standard deviation of the horizontal permeability parallel to the paleo-flow direction.

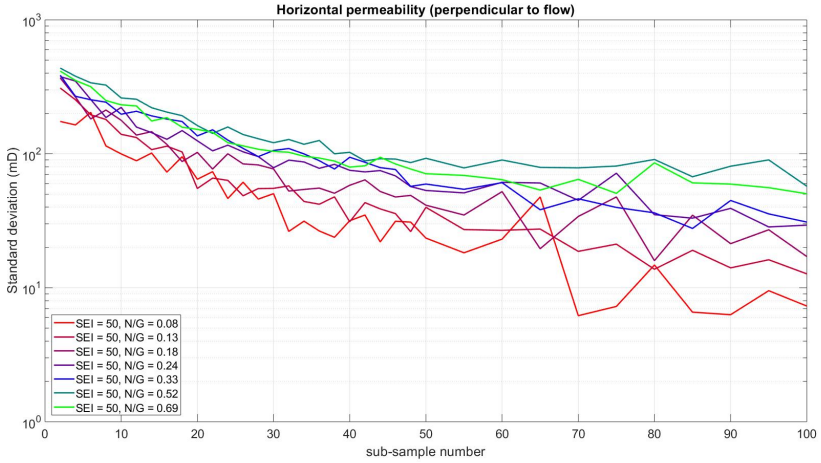

(b) The standard deviation of the horizontal permeability perpendicular to the paleo-flow direction.

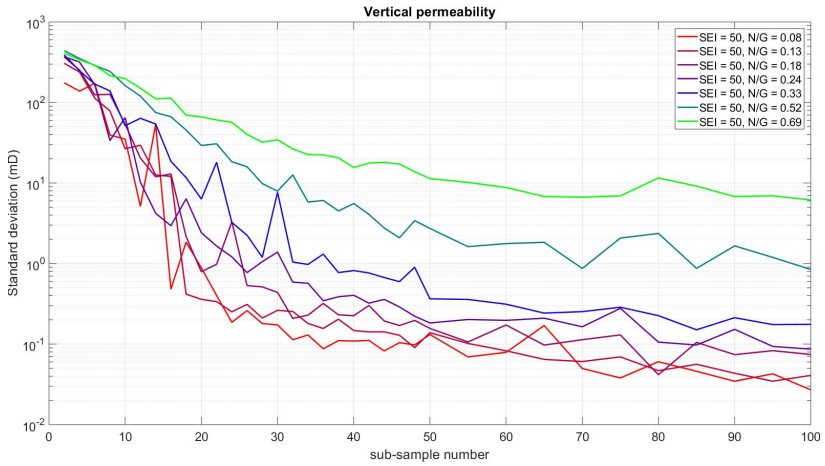

(c) The standard deviation of the vertical permeability.

Figure B.4: The standard deviation of the permeability as a function of sample volume for models with a Sandbodies Extension Index of: 50.

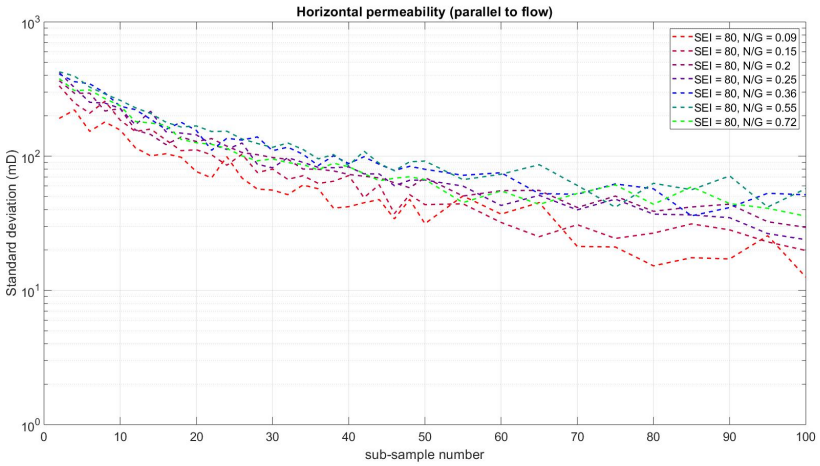

(a) The standard deviation of the horizontal permeability parallel to the paleo-flow direction.

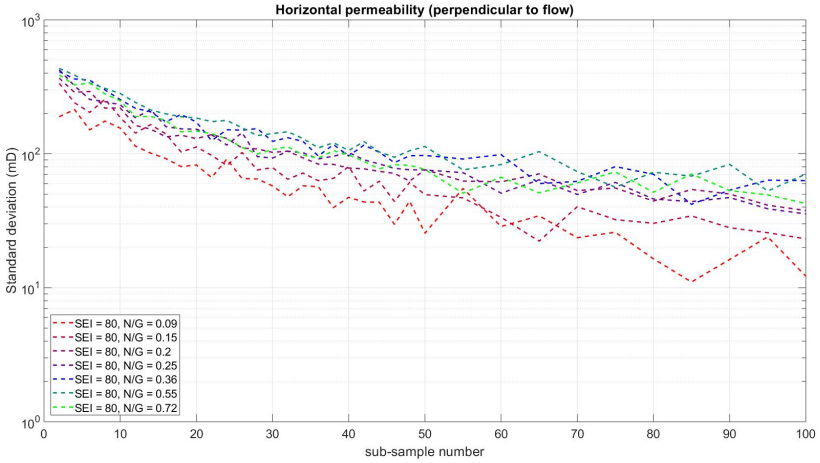

(b) The standard deviation of the horizontal permeability perpendicular to the paleo-flow direction.

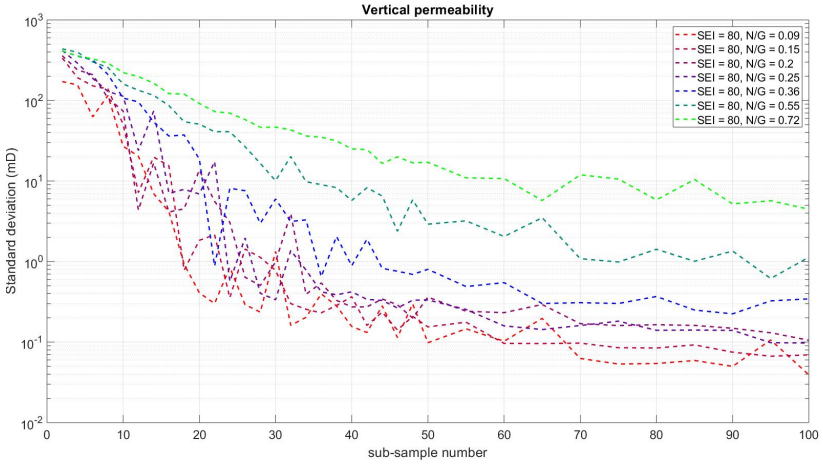

(c) The standard deviation of the vertical permeability.

Figure B.5: The standard deviation of the permeability as a function of sample volume for models with a Sandbodies Extension Index of: 80.

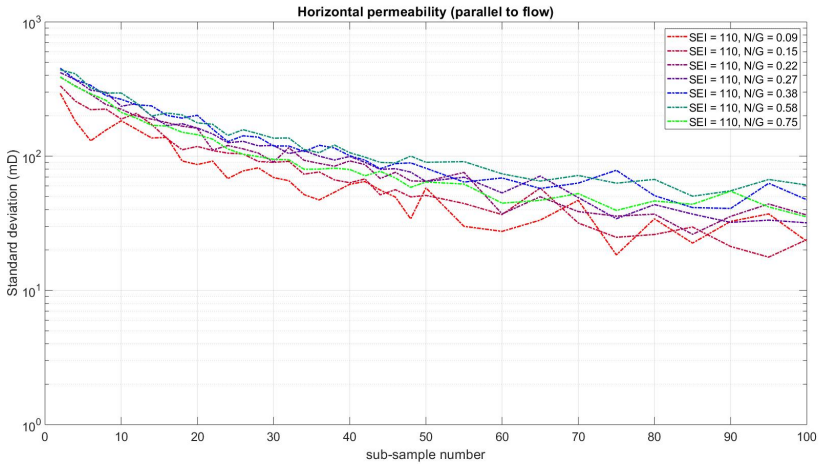

(a) The standard deviation of the horizontal permeability parallel to the paleo-flow direction.

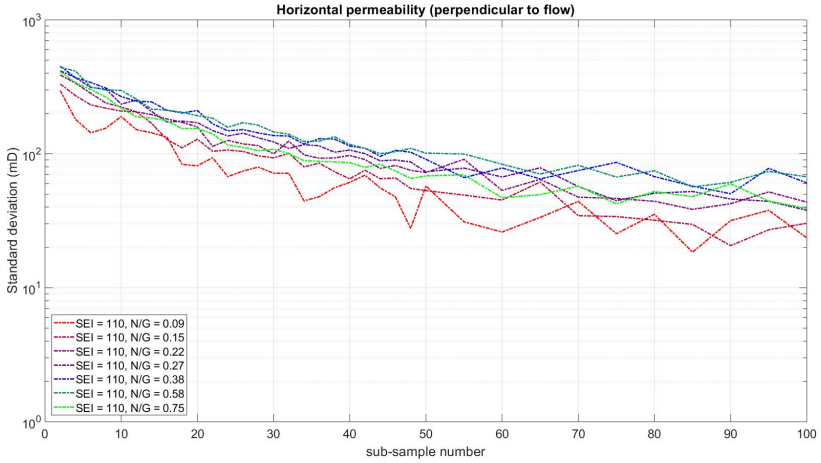

(b) The standard deviation of the horizontal permeability perpendicular to the paleo-flow direction.

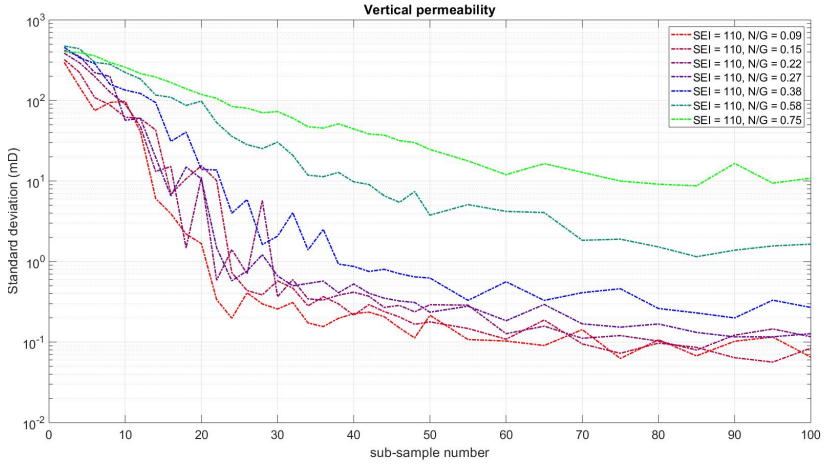

(c) The standard deviation of the vertical permeability.

Figure B.6: The standard deviation of the permeability as a function of sample volume for models with a Sandbodies Extension Index of: 110.

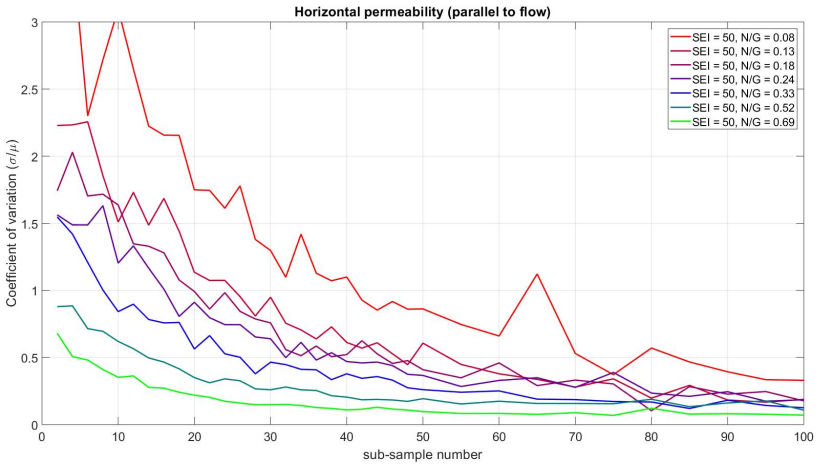

(a) The coefficient of variation of the horizontal permeability parallel to the paleo-flow direction.

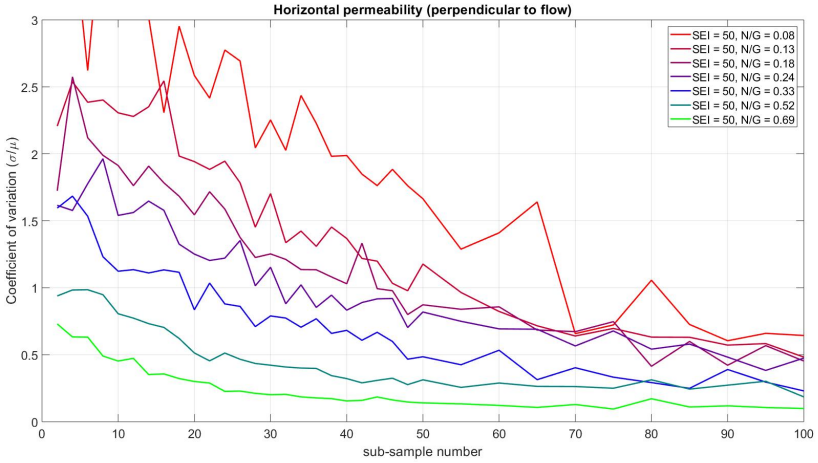

(b) The coefficient of variation of the horizontal permeability perpendicular to the paleo-flow direction.

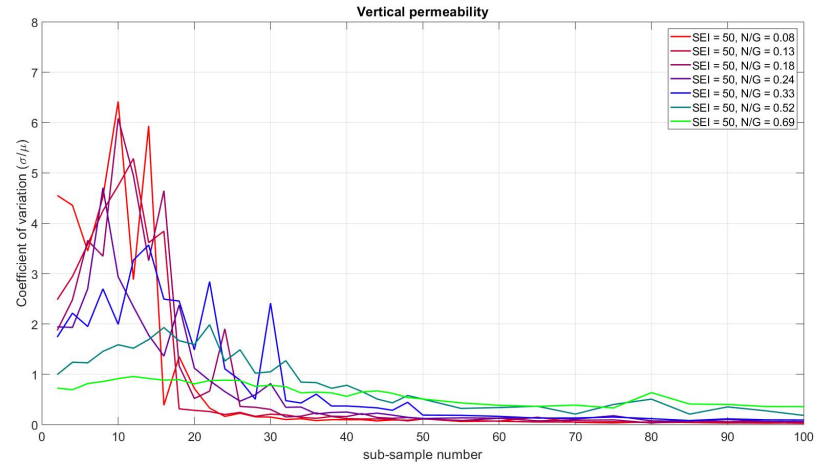

(c) The coefficient of variation of the vertical permeability.

Figure B.7: The coefficient of variation of the permeability as a function of sample volume for models with a Sandbodies Extension Index of: 50.

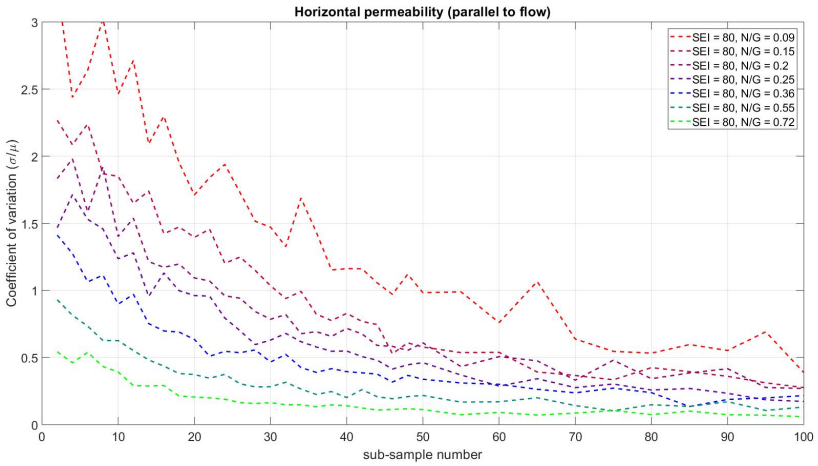

(a) The coefficient of variation of the horizontal permeability parallel to the paleo-flow direction.

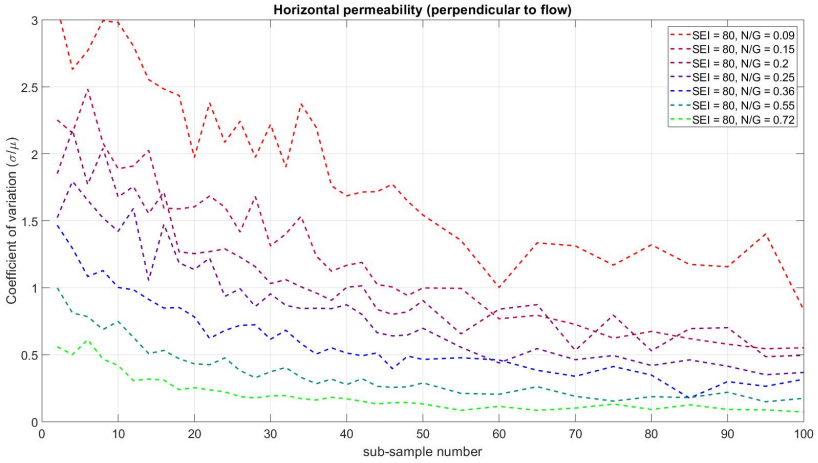

(b) The coefficient of variation of the horizontal permeability perpendicular to the paleo-flow direction.

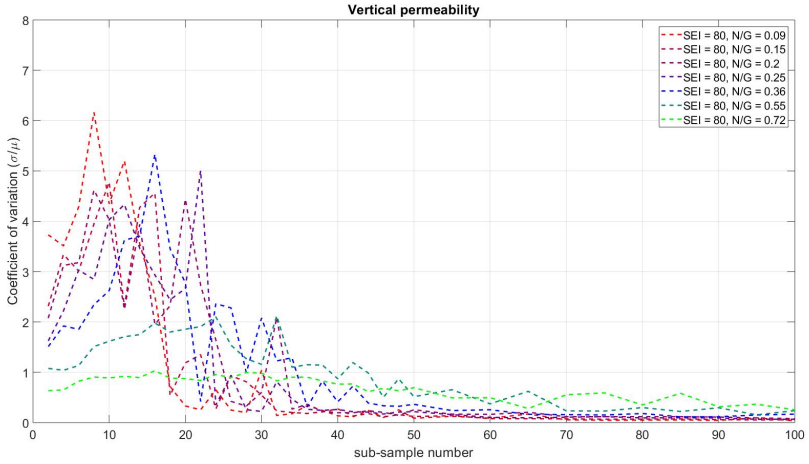

(c) The coefficient of variation of the vertical permeability.

Figure B.8: The coefficient of variation of the permeability as a function of sample volume for models with a Sandbodies Extension Index of: 80.

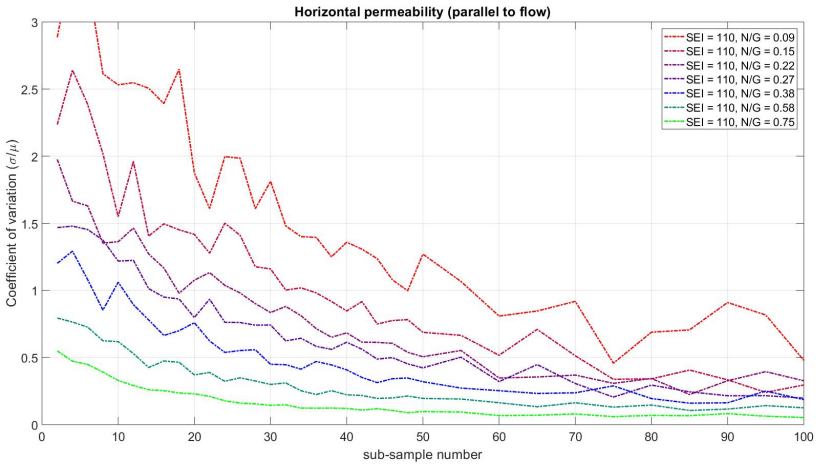

(a) The coefficient of variation of the horizontal permeability parallel to the paleo-flow direction.

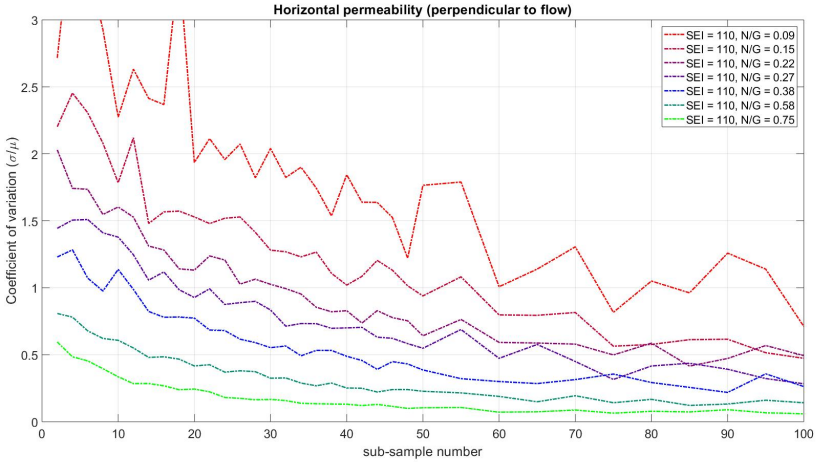

(b) The coefficient of variation of the horizontal permeability perpendicular to the paleo-flow direction.

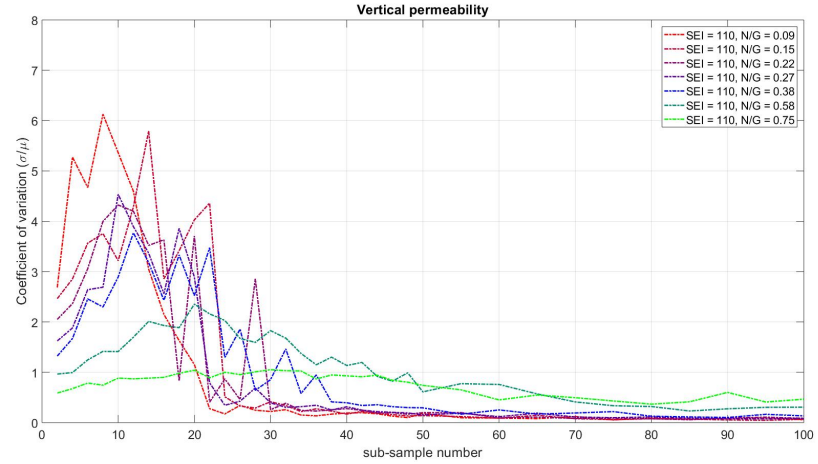

(c) The coefficient of variation of the vertical permeability.

Figure B.9: The coefficient of variation of the permeability as a function of sample volume for models with a Sandbodies Extension Index of: 110.

C DIMENSIONLESS MEAN DIFFERENCE WITH THE 'TRUE' EFFECTIVE PERMEABILITY

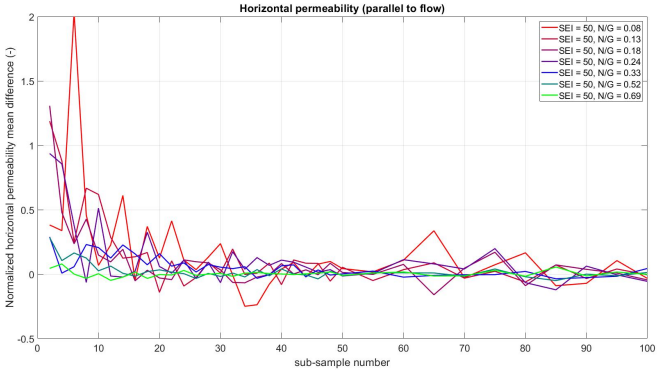

(a) The dimensionless mean difference between the horizontal permeability parallel to the paleo-flow direction and mean of the horizontal permeability parallel to the paleo-flow direction between sub-sample number 90 and 100 as a function of sample volume.

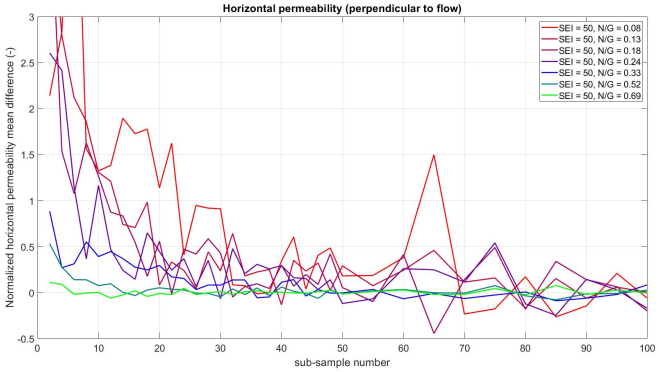

(b) The dimensionless mean difference between the horizontal permeability perpendicular to the paleo-flow direction and mean of the horizontal permeability perpendicular to the paleo-flow direction between sub-sample number 90 and 100 as a function of sample volume.

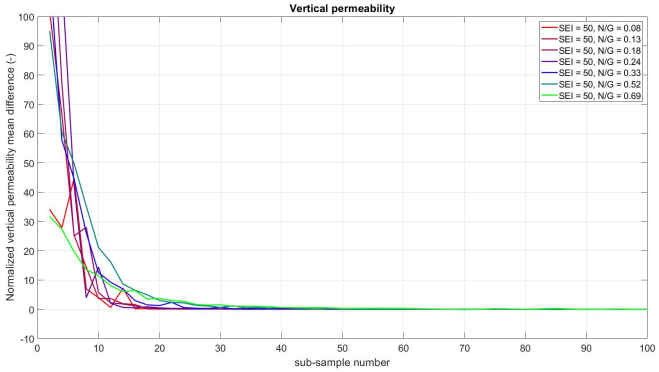

(c) The dimensionless mean difference between the vertical permeability and mean of the vertical permeability between sub-sample number 90 and 100 as a function of sample volume.

Figure C.1: The dimensionless mean difference between the permeability and mean of the permeability between sub-sample number 90 and 100 as a function of sample volume for models with a Sandbodies Extension Index of: 50.

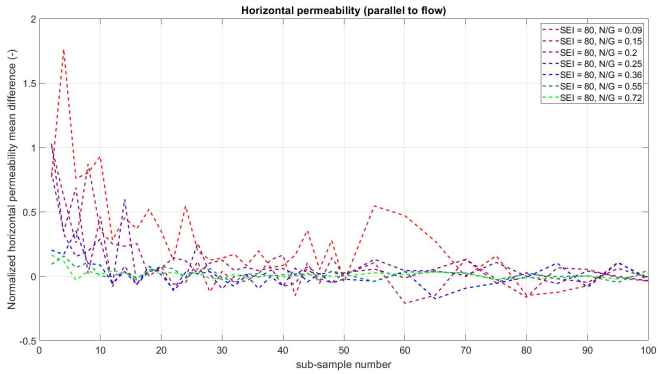

(a) The dimensionless mean difference between the horizontal permeability parallel to the paleo-flow direction and mean of the horizontal permeability parallel to the paleo-flow direction between sub-sample number 90 and 100 as a function of sample volume.

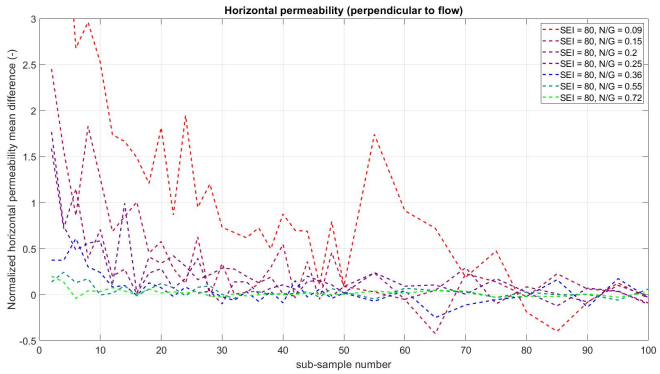

(b) The dimensionless mean difference between the horizontal permeability perpendicular to the paleo-flow direction and mean of the horizontal permeability perpendicular to the paleo-flow direction between sub-sample number 90 and 100 as a function of sample volume.

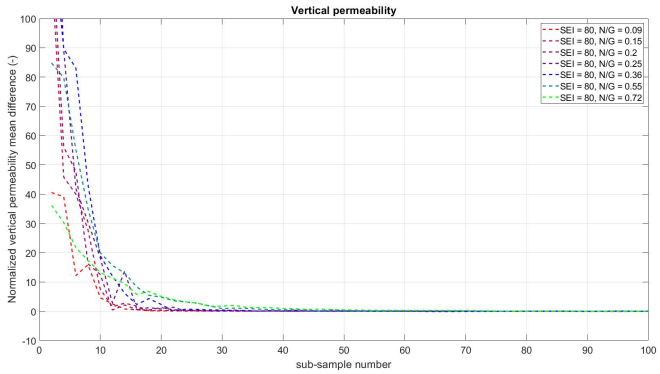

(c) The dimensionless mean difference between the vertical permeability and mean of the vertical permeability between sub-sample number 90 and 100 as a function of sample volume.

Figure C.2: The dimensionless mean difference between the permeability and mean of the permeability between sub-sample number 90 and 100 as a function of sample volume for models with a Sandbodies Extension Index of: 80.

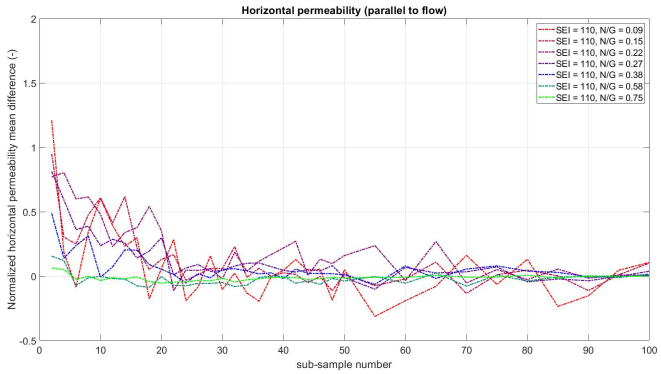

(a) The dimensionless mean difference between the horizontal permeability parallel to the paleo-flow direction and mean of the horizontal permeability parallel to the paleo-flow direction between sub-sample number 90 and 100 as a function of sample volume.

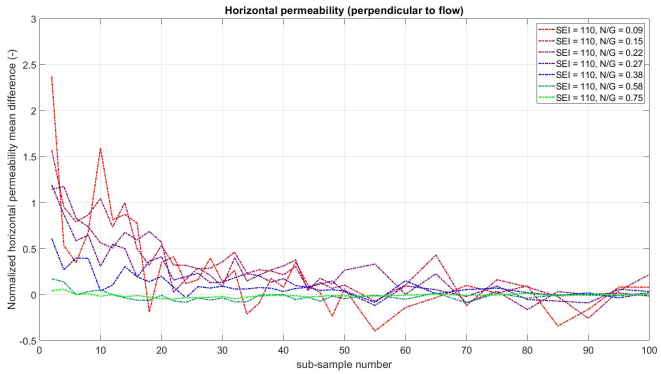

(b) The dimensionless mean difference between the horizontal permeability perpendicular to the paleo-flow direction and mean of the horizontal permeability perpendicular to the paleo-flow direction between sub-sample number 90 and 100 as a function of sample volume.

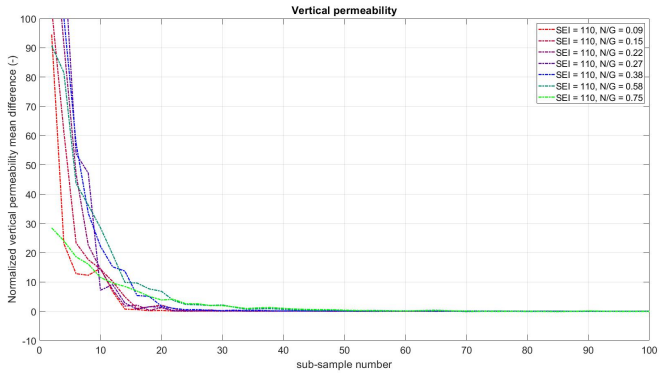

(c) The dimensionless mean difference between the vertical permeability and mean of the vertical permeability between sub-sample number 90 and 100 as a function of sample volume.

Figure C.3: The dimensionless mean difference between the permeability and mean of the permeability between sub-sample number 90 and 100 as a function of sample volume for models with a Sandbodies Extension Index of: 110.

COLOPHON

This document was typeset using LaTeX. The document layout was generated using the `arsclassica` package by Lorenzo Pantieri, which is an adaption of the original `classicthesis` package from Andr Miede.